CHALMERS
UNIVERSITY OF TECHNOLOGY

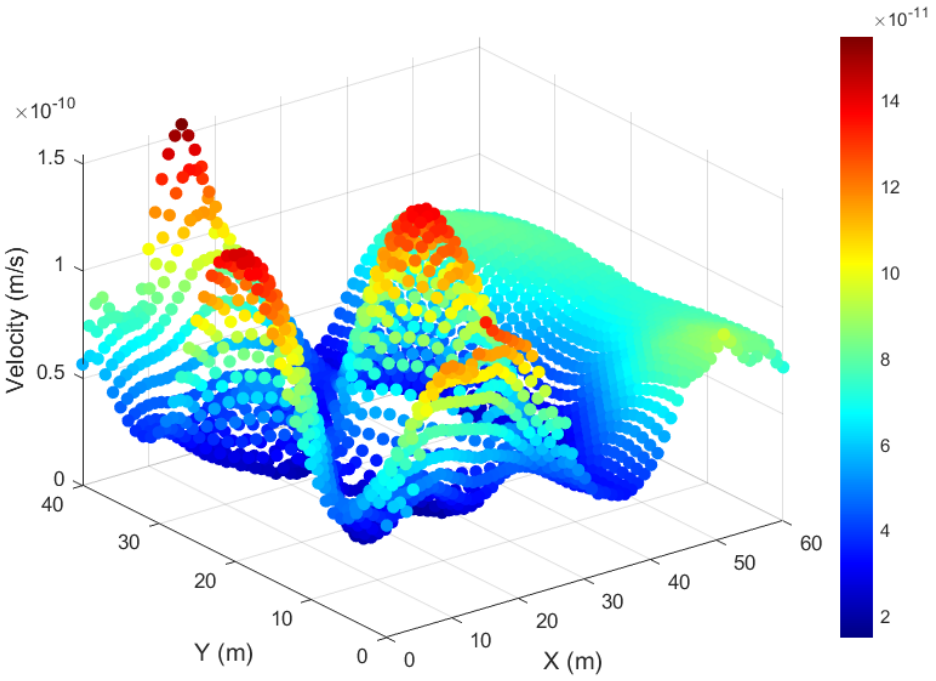

Investigation of Ground Borne Noise Transmission by Numerical Simulation

Master's thesis in Sound and Vibration

Reza Sajadi

DEPARTMENT OF ARCHITECTURE AND CIVIL ENGINEERING

Chalmers University of Technology
Gothenburg, Sweden 2025
www.chalmers.se

Master's thesis 2025

Investigation of Ground Borne Noise Transmission by Numerical Simulation

REZA SAJADI

DEPARTMENT OF ARCHITECTURE AND CIVIL ENGINEERING
Division of Applied Acustics
Chalmers University of Technology
Gothenburg, Sweden 2025

Investigation of Ground Borne Noise Transmission by Numerical Simulation
Numerical modeling of vibration propagation from underground tunnels in bedrock
Reza Sajadi

Examiner: Associate Professor Patrik Höstmad
Supervisor: Doctoral Student Fatemeh Dashti

Master's Thesis 2025
Department of Architecture and Civil Engineering
Division of Applied Acoustics
Chalmers University of Technology
SE-412 96 Gothenburg
Telephone +46 31 772 1000

Cover: [Cover: 3D Matlab scatter plot showing the simulated ground surface velocity at 200 Hz when a train passes through a single underground tunnel. The color scale (jet colormap) indicates the magnitude of the velocity blue areas represent lower vibration levels, and red areas represent higher vibration levels.]

Typeset in LaTeX
Printed by Chalmers Reproservice
Gothenburg, Sweden 2025

Abstract

Ground borne noise and vibrations from underground railway tunnels can pose significant challenges in urban environments, negatively affecting the quality of life of nearby residents. This thesis investigates the transmission of ground-borne vibration from underground railway tunnels in bedrock, with a focus on the influence of fracture zones, tunnel geometry, and model dimensionality. The aim is to improve understanding of how vibrations propagate through stiff geological media and how the resulting vibrations at the surface are affected by subsurface inhomogeneities.

A series of numerical simulations were carried out using COMSOL Multiphysics in both 2D and 3D, analyzing single and twin tunnel configurations under various conditions. Special attention was given to the presence of vertical fracture zones, which were modeled as weakened regions within the rock mass. The effect of tunnel depth and structural layout was also examined. In addition, a parametric study was conducted to determine which material properties of the fracture zones affect the most the wave propagation.

Simulation results showed that when vibration travels from the source through the fracture zone, attenuation increases significantly at the ground surface beyond the fractures, especially at mid-to-high frequencies (250-800 Hz). Tunnel depth and geometry were also found to influence surface vibration levels, with deeper tunnels and certain twin tunnel configurations reducing amplitudes. Both 2D and 3D simulations exhibited similar trends in how frequency influenced the results. However, the 3D model, by incorporating the third spatial dimension, provided a more realistic representation and captured greater spatial detail in how the effects varied across the environment.

The findings were compared with site measurements conducted above an operational railway tunnel. The measurements confirmed key simulation trends, including the dominant frequency range and the general decay of vibration levels with distance.

Keywords: Ground-borne vibration, underground railway, fractured bedrock, COMSOL Multiphysics, 2D/3D simulation, twin tunnel geometry, frequency analysis.

Acknowledgements

Most of all, I would like to offer my sincere thanks to my supervisor, Fatemeh Dashti, for her continuous guidance and encouragement throughout my thesis. Her guidance in the process of simulation and data collection was also greatly helpful. I am also extremely grateful to my examiner Patrik Höstmad for his regular discussions, constructive criticism, and encouragement, which kept me focused and motivated throughout the project.

This thesis was done at Chalmers University of Technology, Division of Applied Acoustics. I am thankful for the study conditions and equipment available, which made this possible. The topic is related to the research project "Methodology to Refine Prediction of Ground Borne Noise" funded by the Swedish Transport Administration (Trafikverket). I appreciate their contribution to inspiring the topic.

To my fellow students, your hospitality, discussions, and encouragement created a welcoming and stimulating study environment that I will always value.

Lastly, I would like to thank my family and friends. Your encouragement, patience, and emotional support have made all the difference along this way.

Reza Sajadi Gothenburg, May 2025

Contents

List of Figures

Chapter 1

Introduction

Noise and vibration impacts from underground railways are part of the broader environmental impact in Europe [8], significantly affecting the quality of life of those living close to the railway routes. Documented health effects include sleep disturbance, annoyance, and an increased risk of ischemic heart disease (IHD) and hypertension [**11**, 8]. As a train moves underground, it generates vibrations that travel through the surrounding ground. These vibrations cause the ground to oscillate, and when they encounter different materials or nearby structures, they can potentially cause damage [14], disturbing vibrations and audible ground borne noise [20].

This project focuses mainly on ground-borne noise generated by underground trains. The vibration comes from train wheels moving on tracks; these vibrations travel underground and can transfer to nearby buildings. This causes building elements such as floors, ceilings, and walls to become secondary sources, producing audible noise inside the building [20]. According to the Swedish trasport administration's guildeline, the maximum allowed indoor noise level is $32\,\mathrm{dB(A)}_{\mathrm{F,max}}$ (A-weighted sound pressure level with Fast time weighting), and the vibration level should not exceed $4\,\mathrm{mm\,s^{-1}}_{w,\mathrm{rms}}$ (comfort-weighted root mean square velocity with Slow time weighting) inside residential apartments [18].

So studying ground borne noise transmission from railways is essential for human well being, structure safety, environmental protection. The planner must ensure that noise is taken into account when choosing the right location to build a subway for more sustainable urban development while advancing railway technology with minimal disruption to the communities.

1.1 Aim

A model has been developed in collaboration with The Swedish Transport Administration that can predict ground-borne noise [9]. In this M.Sc. project numerical simulations are used to investigate specific scenarios to improve the existing model. Scenarios include cracked zones, special bedrock geometries, and multiple tunnel configurations. The results of the simulations will then be compared with the field measurement data. Finally, after analyzing

all the data and models, the project aims to provide generalized conclusions applicable to specific cases to improve the ground-borne noise model by new correction terms.

1.2 Objectives

The objective of this thesis is to investigate of how vibrations at the ground surface are affected when various inhomogeneities are present in the ground. The results could potentially be used to improve the accuracy and applicability of an existing ground-borne noise prediction model. To achieve this, numerical simulations are conducted using COMSOL Multiphysics to model vibration propagation from tunnels under varying conditions. The scenarios include different tunnel configurations, such as twin tunnels placed side by side, one above the other, and at 45 degrees. In addition, fractured zones were modeled as simplified regions with reduced stiffness and density, and single- and multiple-cracker zones with varying areas were studied to observe their impact on underground vibration behavior.

1.3 Limitations

The following limitations were identified in this study:

- Numerical simulations were limited to calculating vertical particle velocity. Horizontal and rotational components were not considered. This simplification was made because vertical ground vibrations are typically more significant for both human perception and structural response. Moreover, the vibration sensors used to estimate acceleration levels are designed to measure vertical motion[7].
- The tunnel was modeled as embedded in typical Swedish bedrock. No overlying soft soils or groundwater effects were included.
- A simplified fractured zone was modeled as a weaker, dry region with no gas content. It was assumed to behave as a linear elastic material.
- Complex features such as fracture orientation, connectivity, and nonlinear behavior—common in real-world scenarios—were not included. This simplification was motivated by the need to reduce modeling and computational time in COMSOL.
- Site-specific mismatch: The Gårda tunnel does not have a twin tunnel, and there is no confirmed data on the presence of vertical fracture zones at the site. Therefore, some of the simulated scenarios are hypothetical and were included to explore general effects rather than replicate exact site conditions.

Chapter 2

Theory

To accurately model and interpret ground borne noise and vibration from underground railways, it is essential to understand the physical principles that govern wave propagation in geological media. This chapter presents the theoretical foundation needed to support the numerical modeling and analysis carried out in this thesis.

The first section introduces the main types of waves generated by tunnel-based train activity, as their behavior, particularly how they propagate and attenuate, has a direct impact on how vibrations reach the surface and affect nearby structures. Following this, the concept of damping is discussed to explain how the wave energy decreases due to material and geometric factors, both of which are critical in evaluating vibration amplitudes over distance. Given that the surrounding medium in this study is fractured rock, a separate section addresses wave behavior in rock masses, highlighting how fracture zones influence reflection, refraction, and wave transmission. A clearer understanding of these phenomena is necessary to evaluate the effect of rock quality and fracture conditions on the spread of vibrations.

Finally, the chapter outlines the numerical methods used in this research, particularly the Finite Element Method (FEM), and explains the implementation of Perfectly Matched Layers (PML) to simulate an infinite domain. These numerical tools are central to the modeling strategy used in COMSOL Multiphysics, making it important to provide a theoretical basis for their use.

2.1 Type of waves

Seismic waves that travel through the ground are generally divided into two main types: **body waves** and **surface waves**:

Body waves are seismic waves that travel through the interior of a ground medium, such as soil or rock. They are classified into two main types: **P-waves** and **S-waves**.

- **P-waves** (primary or pressure waves) are longitudinal seismic waves in which particle motion is parallel to wave propagation. Their velocity depends on the material properties of the ground, particularly the *elastic modulus* and *density*. Specifically, higher

stiffness (modulus) increases the P-wave speed, while higher density reduces it. As described by equation 2.1:

$$C_P = \sqrt{\frac{E\,(1-\nu)}{\rho\,(1-2\nu)\,(1+\nu)}} \tag{2.1}$$

where:

- C_P is the P-wave velocity,
- E is Young's modulus,
- ν is Poisson's ratio,
- ρ is the ground density.

- **S-waves** (shear waves) are the second fastest type of body wave. They propagate in a direction *perpendicular* to the motion of the medium, causing side-to-side or vertical shearing motion [20]. Their velocity is expressed in equation 2.2.

$$C_S = \sqrt{\frac{E}{2\,\rho\,(1+\nu)}} \tag{2.2}$$

where:

- C_S is the S-wave velocity,
- E is Young's modulus,
- ρ is the ground density,
- ν is Poisson's ratio.

Surface Waves

Rayleigh waves are surface waves that travel along the ground surface. This motion rotates the surface in the opposite direction of the wave's travel. In tunnel environments, when body waves (P-waves and S-waves) reach the surface, they can partly convert into Rayleigh waves [20] [3]. It is explained by equation 2.3:

$$C_R \approx \frac{0.87 + 1.12\,\nu}{1+\nu}\,C_S \tag{2.3}$$

where:

- C_R is the Rayleigh wave velocity,
- ν is Poisson's ratio,
- C_S is the S-wave velocity.

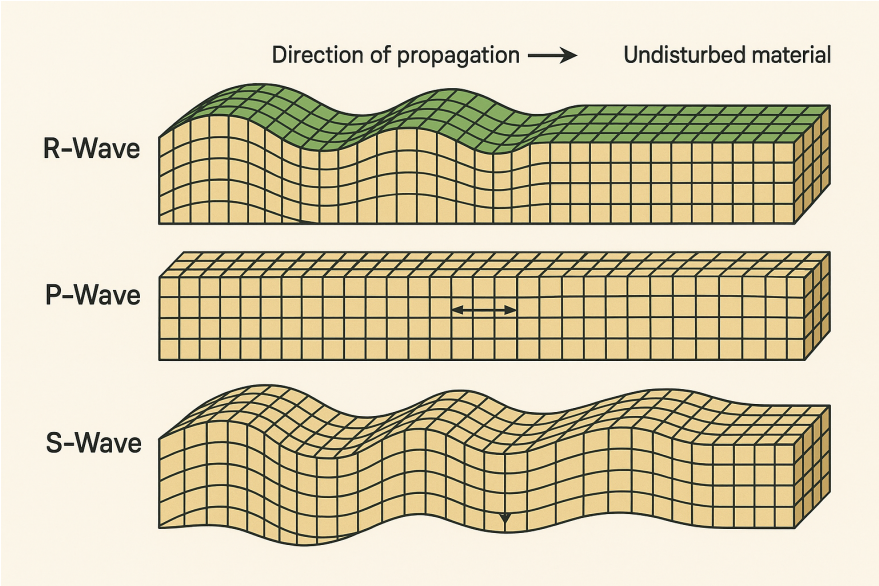

Figure 2.1: Different Types of Ground Waves, Adapted from International union of Railways UIC [20]

2.2 Damping

Vibrational waves traveling through bedrock experience two primary forms of damping: geometrical and material. Geometrical damping describes how the wave amplitude reduces because the energy spreads over a larger volume with distance. For instance, surface waves dominate farther from the source, as their geometrical attenuation is less than that of body waves. Lamb's equation captures this effect 2.4:

$$v = v_1 \left(\frac{r_1}{r}\right)^m, \tag{2.4}$$

where v is the amplitude at distance r, v_1 is the amplitude at reference distance r_1, and m is an exponent depending on the wave type and source 2.1.

Table 2.1: Values of the constant m for different wave types and source geometries [16]

Wave Type	**Point Source**	**Line Source**
P-wave	1.0	0.5
S-wave	1.0	0.5
R-wave	0.5	0.0

Material damping, on the other hand, results from internal friction within the bedrock, causing energy loss during each cycle of deformation. This additional dissipation can be

incorporated into Lamb's equation via an exponential term, often referred to as Bornitz's extension:

$$v = v_1 \left(\frac{r_1}{r}\right)^m e^{-\alpha(r-r_1)}, \tag{2.5}$$

where α is the material damping coefficient [12]. Higher values of α indicate faster energy dissipation due to factors such as looser soil and higher vibration frequency. Consequently, low-frequency vibrations in stiff bedrock of high quality can travel relatively far, while higher frequencies tend to be more attenuated. Typical material damping values at 50 Hz range from about 0.3 m^{-1} for soft soils to less than 0.003 m^{-1} for stiff bedrock [9].

Table 2.2: Values of damping coefficient for 50 Hz [21].

Soil class	**Damping coefficient** α (1/m)
Soft soils like loose clay	0.1–0.3
Firm soils like solid clay	0.03–0.1
Stiff soils like very stiff clay	0.003–0.03
Stiff bedrock	<0.003

2.3 Reflection and refraction

Reflection and refraction occur when a wave facing an interface between two different materials. Reflection is the return of part of the wave energy into the original medium, while refraction is the change in wave direction as it passes into a material with a different wave speed. In rock mechanics, these phenomena occur at interfaces between materials with different seismic velocities or at discontinuities such as joints or fractures. The behavior of reflected and refracted waves is governed by Snell's Law, where the angle of incidence, velocity contrast, and wave frequency determine the energy partition. Even when seismic velocities are the same on both sides of an interface, imperfect bonding due to joint roughness, infill, or weathering can still cause wave reflection and refraction. If the interface is perfectly bonded, wave scattering does not occur, making the boundary effectively invisible . Joint stiffness also plays a key role: low-stiffness joints reflect more energy, while high-stiffness joints transmit more. Higher-frequency waves tend to reflect more than lower-frequency ones [10].

2.4 Wave Propagation in Rock Masses

Wave propagation in rock masses is influenced by the physical properties of the material, the presence of discontinuities, and the geometry of the subsurface. As stress waves (e.g., P-waves, S-waves) travel through rock, they experience attenuation due to internal friction and material damping. In addition, the presence of joints and fractures increases attenuation due to seismic impedance contrasts between geological regions, which causes reflection and refraction at interfaces [13, 5].

Wave *frequency* (or wavelength) also plays a critical role. High-frequency waves (short wavelength) tend to be mostly reflected, while low-frequency waves (long wavelength) are more likely to be transmitted across a discontinuity [13, 5].

The influence of a single discontinuity on wave propagation depends on several parameters:

- Surface roughness,
- Type and thickness of infill material,
- Aperture (opening) of the discontinuity,
- Compressive strength of contact surfaces,
- Normal and shear stiffness,
- Water pressure and flow.

These factors affect the mechanical contact across the interface, thereby altering reflection, transmission, and mode conversion. Water, in particular, can increase the aperture, facilitate chemical weathering, or introduce weak infill material, all contributing to reduced wave transmission [19].

In natural rock masses, discontinuities often appear in sets with dominant orientations and spacings. When randomly distributed, it is difficult to model each discontinuity individually. Thus, the rock mass is often treated as an equivalent continuous medium, with reduced stiffness approximated using classification systems such as the Rock Mass Rating (RMR) [4] or the Q-system [1].

When rock masses are intersected by multiple parallel discontinuities, wave propagation becomes more complex due to repeated reflection and refraction at each interface [22]. Analytical models addressing these effects have been developed by several researchers [13, 6, 22].

The Displacement Discontinuity Model (DDM) was applied to calculate reflection and transmission coefficients across a single discontinuity, accounting for stiffness and impedance contrasts [13]. The model applies to both dry and saturated joints and accommodates arbitrary angles of incidence. For multiple discontinuities, the model assumes equal stiffness and identical seismic impedance across joints, ignoring inter-joint reflections. Therefore, it is valid only when joint spacing is significantly larger than the wavelength. When the wavelength of the wave is comparable to the spacing between joints, multiple reflections occur between the joints. These reflected waves overlap and interfere with each other, producing a composite transmitted wave through superposition [22]. To model this behavior, the method of characteristics was used to extend the analysis, enabling the prediction of particle velocity and stress on both sides of the joints. This extended model accounts for joint spacing, joint stiffness, and wave frequency [6].

2.5 Numerical Methods for Investigating Ground-Borne Noise Transmission

Numerical simulation plays a central role in understanding and predicting ground-borne vibration propagation from underground railway tunnels, especially in conditions where analytical or semi-analytical models are insufficient. Analytical methods often assume idealized geometries and homogeneous ground conditions, limiting their applicability in real-world environments such as fractured rock masses or layered soil [17].

2.5.1 The Finite Element Method (FEM)

The Finite Element Method (FEM) is a powerful numerical technique widely used to solve partial differential equations (PDEs), particularly suited for analyzing complex geometries and heterogeneous media. FEM involves discretizing the computational domain into a mesh composed of smaller subdomains, known as elements. Each element is governed by specific equations derived from fundamental physical principles, such as elasticity theory in structural dynamics. The overall response of the system is then captured by assembling the individual element matrices into global matrices [17].

For dynamic analyses, FEM is extended by incorporating matrices that account for inertia and damping effects. The dynamic equilibrium equation commonly employed in FEM vibration analysis is expressed as 2.6:

$$\mathbf{M}\ddot{\mathbf{u}}(t) + \mathbf{C}\dot{\mathbf{u}}(t) + \mathbf{K}\mathbf{u}(t) = \mathbf{F}(t) \tag{2.6}$$

where:

- $\mathbf{M}$ is the global mass matrix, representing inertial effects,
- $\mathbf{C}$ is the global damping matrix, capturing energy dissipation mechanisms,
- $\mathbf{K}$ is the global stiffness matrix, reflecting the structural stiffness of the system,
- $\mathbf{u}(t)$ is the displacement vector at time t,
- $\dot{\mathbf{u}}(t)$ and $\ddot{\mathbf{u}}(t)$ are the velocity and acceleration vectors, respectively,
- $\mathbf{F}(t)$ is the external dynamic load vector.

This formulation enables detailed time-domain analyses of structural responses under transient dynamic loads, such as those induced by train wheel-rail interactions. Damping, crucial for realistic simulations, can be introduced using various methods, including Rayleigh damping models [15].

2.5.2 Modeling Infinite Domains with PML

One of the fundamental challenges in wave propagation modeling using FEM is the treatment of boundaries. Since the real domain is effectively infinite, truncating the domain in numer-

ical models can cause artificial reflections at the edges, leading to non-physical results. To mitigate this, Perfectly Matched Layers (PMLs) are implemented as non-reflecting absorbing boundaries[11].The PML technique, introduced by Berenger (1994), works by applying a complex coordinate stretching transformation in a designated absorbing layer [2].

In numerical simulations of ground-borne vibrations, the excitation is typically applied at a single point in both two-dimensional (2D) and three-dimensional (3D) models. However, due to the difference in dimensionality, this source represents different physical conditions. In a two-dimensional (2D) model, a point excitation corresponds to an *coherent line source*, implying continuous energy input along an infinite line perpendicular to the model plane. In contrast, a three-dimensional (3D) model allows the source to represent a true *point source*.

Chapter 3

Methodology

This chapter describes the methodology employed to investigate the transmission of ground-borne noise and vibration from an underground railway tunnel. The study integrates numerical modeling using COMSOL Multiphysics with in-situ measurement data to better understand the propagation of vibrations through the ground and their attenuation characteristics.

In-situ measurements were carried out at the Gårda tunnel site. Decay measurements were performed on the ground surface above the tunnel to obtain insights into the attenuation behavior of vibrations as they propagate through the bedrock.

The methodology is structured into three main parts. First, the section on **fractures in bedrock** discusses the modeling approach and assumptions related to fractured geological media, emphasizing how fractures influence wave propagation mechanisms. Second, the **tunnel modeling** section presents the development of both **2D** and **3D finite element simulations** aimed at analyzing the vibration transmission from the tunnel to the ground surface. These models incorporate simplified tunnel geometry and assumed material properties, selected to approximate realistic values for typical underground conditions and to enable a reasonable estimation of the dynamic response. Finally, the **site measurements** section provides an overview of the field measurements conducted at the Gårda tunnel and their role in validating and comparing the numerical simulation results.

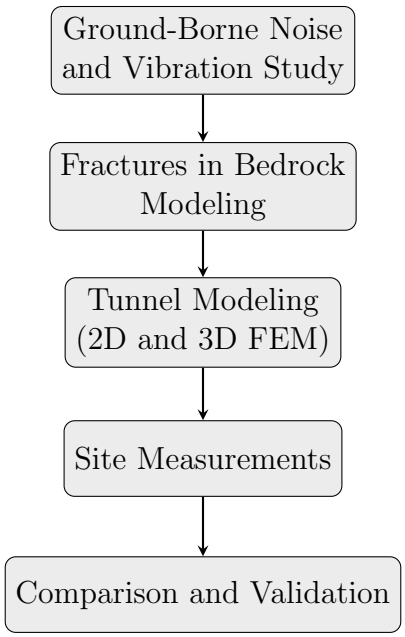

Figure 3.1: Overview of the methodology structure for ground-borne noise and vibration analysis.

3.1 Fracture in Bedrock

Fractures in the bedrock can significantly influence the transmission of ground-borne vibrations by altering local stiffness and introducing wave scattering effects. In this study, fractures are modeled in COMSOL Multiphysics as weakened vertical zones with modified mechanical properties compared to the surrounding intact rock.

These fractured zones are represented as vertical rectangular regions extending from the ground surface to the bottom boundary of the simulation domain, each with an initial width of 2 m. Two scenarios are considered: one with a single vertical fracture, and another with a group of closely spaced fractures representing a fracture-dense zone.

The surrounding ground is assumed to be isotropic and linear elastic, with the following mechanical properties:

- Density: $2400\,\mathrm{kg\,m^{-3}}$
- Young's modulus: $5 \times 10^{10}\,\mathrm{Pa}$
- Poisson's ratio: 0.25
- Isotropic structural loss factor: 0.01

The material properties assigned to the fractured zones are based on reasonable assumptions for open fractures in hard rock. These values are not site-specific but reflect typical conditions found in fractured bedrock. The parameters are defined as follows:

- Density: $1800\,\mathrm{kg\,m^{-3}}$

- Young's modulus: 9×10^8 Pa
- Poisson's ratio: 0.3
- Isotropic structural loss factor: 0.1

To eliminate reflections from the model boundaries and simulate a more realistic, unbounded domain, **PMLs** are applied around the outer edges of the model. This technique effectively absorbs outgoing waves and prevents artificial reflections, allowing the simulation to approximate an infinite ground medium.

The simulations are conducted in two dimensions (2D), assuming plane strain conditions. In this setup, deformation is only allowed in the x and y directions, where x represents the horizontal direction and y represents the vertical direction in the 2D model. A finer mesh is applied in and around the fracture zones to ensure at least five nodes per wavelength, allowing accurate resolution of local variations in stress and displacement fields. Figures showing the model geometry, material zones, and mesh distribution are provided at the end of this section to support the description of the numerical setup 3.2.

To investigate the influence of different fracture geometries on ground-borne vibration transmission, seven configurations were modeled. These configurations vary in terms of fracture number, spacing, and overall width. The considered cases include both isolated and clustered vertical fractures. An overview of these configurations is shown in Figure 3.3.

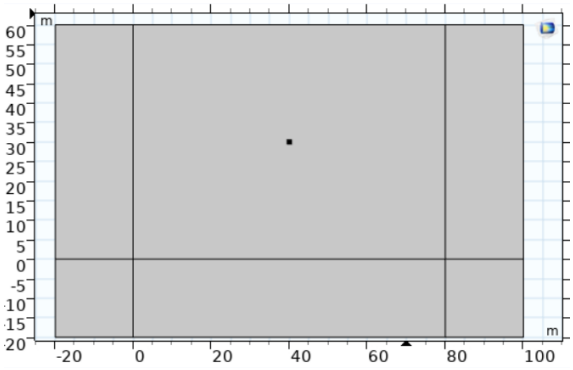

(a) No fracture (reference case)

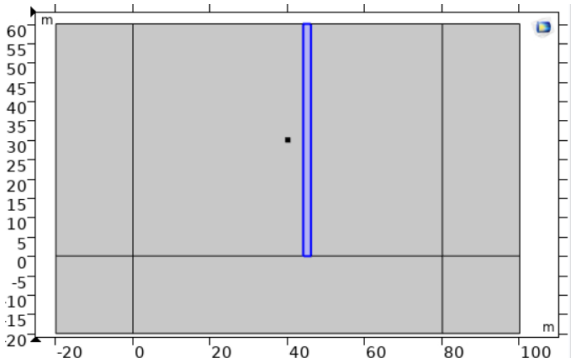

(b) Single fracture, width = 2 m

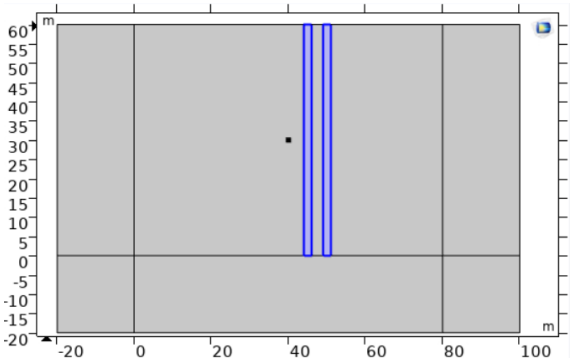

(c) Two fractures, 2 m wide each, 3 m apart

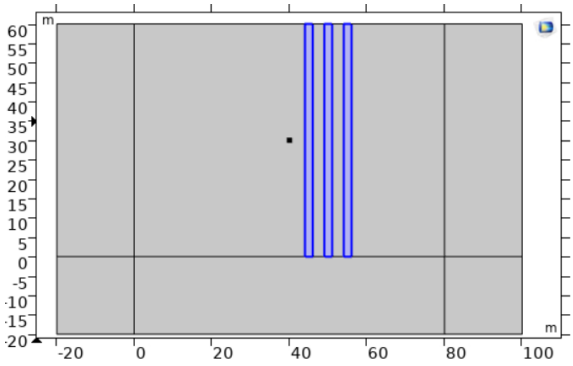

(d) Three fractures in series

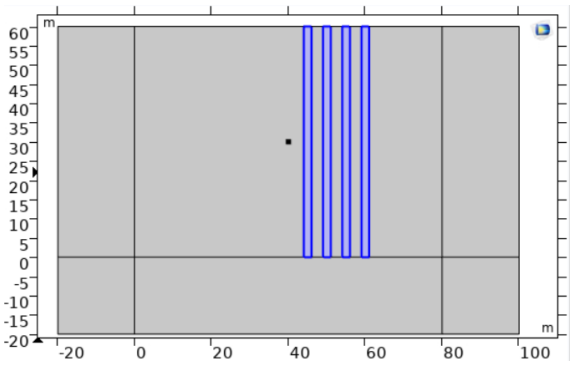

(e) Four fractures in series

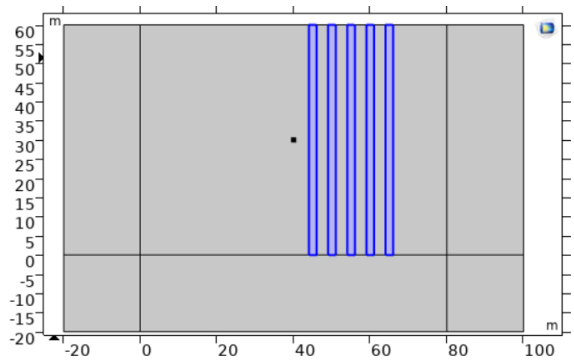

(f) Five fractures in series

Figure 3.2: Fracture configurations (1–6) considered in the numerical simulations.

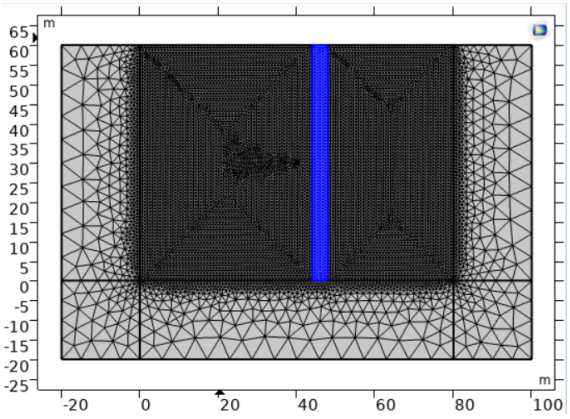

(a) Single wide fracture, width = 4 m with finer element mesh size

Figure 3.3: Fracture configuration (7): single wide fracture.

3.1.1 Parametric study of fracture properties

To better understand which material property of the fractured zone most significantly influences the transmission of ground-borne vibrations, a parametric study was performed. This investigation focused on assessing the relative effect of Young's modulus, density, and Poisson's ratio on surface vibration response.

The model setup was similar to the previous fracture analysis, with a single vertical fracture embedded in homogeneous bedrock. The excitation was applied as a point load underground, and no tunnel cavity was included in this specific study to isolate the material behavior of the fracture. The analysis was conducted in the frequency domain over a range up to 1000 Hz.

The reference fracture material properties were:

- Young's modulus: 9×10^8 Pa
- Density: $1800\,\mathrm{kg\,m^{-3}}$
- Poisson's ratio: 0.3
- Isotropic structural loss factor: 0.1

Three additional simulations were performed, each time modifying one parameter while keeping the others fixed at their reference values: *(1)* increasing Young's modulus to 9×10^9 Pa, *(2)* increasing density to $2200\,\mathrm{kg\,m^{-3}}$, and *(3)* increasing Poisson's ratio to 0.5.

The vibration response was evaluated as vertical velocity at a single surface receiver, using one-third octave band analysis. The results were compared to identify which parameter had the greatest influence on vibration attenuation. The goal was to identify the dominant fracture property affecting wave propagation in simplified ground conditions.

3.2 Tunnel

To study the propagation of ground-borne vibrations from underground railways, a numerical tunnel model was developed using COMSOL Multiphysics. The objective of the tunnel modeling is to simulate wave propagation resulting from a dynamic load, representing the effect of a moving train. The tunnel geometry is designed to resemble the Gårda tunnel in Gothenburg, Sweden, with simplifications to ensure computational efficiency while capturing the essential dynamic behavior.

The tunnel cross-section is circular with a radius of 5 m, and it is embedded in a homogeneous bedrock medium. The surrounding ground is assumed to be isotropic and linear elastic, with the following mechanical properties:

- Density: $2400\,\mathrm{kg\,m^{-3}}$
- Young's modulus: $5 \times 10^{10}\,\mathrm{Pa}$
- Poisson's ratio: 0.25
- Isotropic structural loss factor: 0.01

A point load is applied to the tunnel boundary to simulate the dynamic excitation caused by railway traffic. This loading condition serves to excite wave propagation through the surrounding rock and evaluate the resulting surface and subsurface vibration levels. To maintain a simplified and idealized setup, the tunnel lining and surrounding ground are modeled using constant material properties, and no additional structural layers (e.g., ballast, rail, or sleepers) are included. The simulation domain is surrounded by PMLs to absorb outgoing waves and avoid artificial reflections, allowing the model to approximate an infinite medium.

The detailed setup and modeling strategy are presented in the following subsections, covering both the 2D and 3D simulation approaches.

3.2.1 Numerical simulation in 2D

Two dimensional simulations were performed using the Solid Mechanics interface in COMSOL Multiphysics in the frequency domain. The purpose of the 2D modeling was to reduce computational cost and allow for the investigation of multiple tunnel configurations and fracture scenarios. Both single and twin tunnel cases were analyzed, with the tunnels embedded in homogeneous bedrock. In the twin tunnel case, only one tunnel was subjected to dynamic excitation, while the second tunnel placed at a different depth remained passive to examine interaction effects. A harmonic point load was applied to the tunnel boundary and the response was evaluated in a frequency range of approximately 4 to 800 Hz. Perfectly matched layers (PML) were implemented to minimize boundary reflections. Vibration responses were extracted at selected surface points and along vertical lines above the tunnel(s) to assess how wave propagation is influenced by the tunnel configuration and the presence of fractures.

Single tunnel

The single tunnel scenario was used as a reference case to investigate fundamental vibration propagation in unfractured bedrock. A circular tunnel with a radius of 5 m was embedded at three different depths: 30 m, 40 m, and 50 m below the ground surface. A harmonic point load was applied at the center of the tunnel invert (bottom) to simulate dynamic excitation.

The simulation was conducted in the frequency domain using the Solid Mechanics interface in COMSOL Multiphysics. No fractures were included in this scenario in order to isolate the influence of the tunnel structure and to study wave propagation in a homogeneous medium. The numerical mesh was refined to ensure a minimum of five elements per wavelength up to 800 Hz, allowing for adequate resolution of high-frequency wave content. To avoid boundary reflections and simulate an infinite domain, PMLs were applied around the model boundaries.

The vibration response was evaluated of the vertical velocity at a receiver point located on the ground surface. In addition, average velocity levels were calculated along surface lines directly above the tunnel to analyze both attenuation and spatial distribution of vibration at the surface. Figures below shows the shape and position of the tunnel at three different depths; see Figures 3.4.

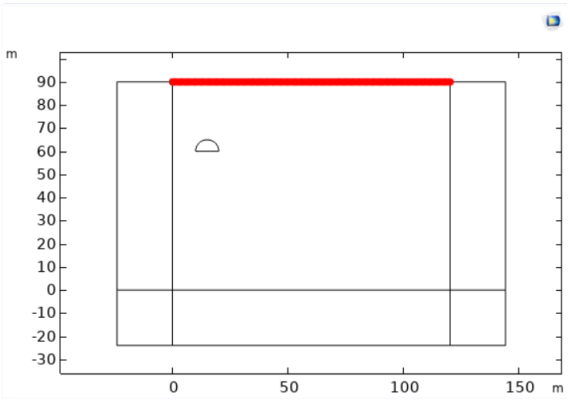

(a) 30 m depth

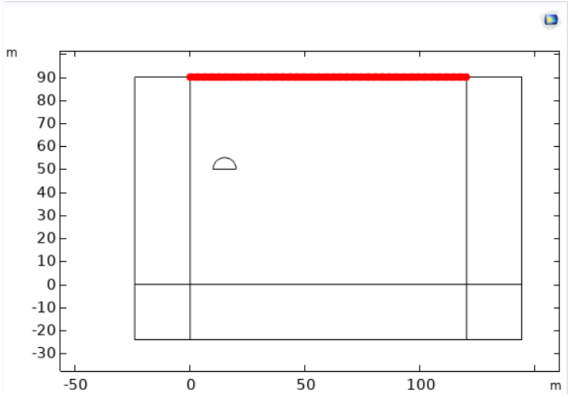

(b) 40 m depth

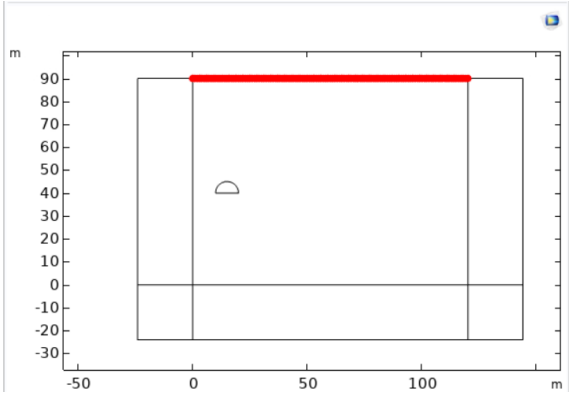

(c) 50 m depth

Figure 3.4: Receiver positions (red line) located on the ground surface at 1 m intervals.

Twin tunnel

The twin tunnel scenario was modeled to investigate the influence of tunnel-tunnel interaction on ground-borne vibration propagation. Both tunnels were circular with a radius of 5 m, and the center-to-center spacing between them was set to 20 m. Several geometric configurations were considered: tunnels placed side by side at the same depth, tunnels offset vertically (one above the other), and tunnels positioned at a 45-degree angle relative to each other. These variations were included to study how tunnel alignment affects vibration shielding or amplification effects at the ground surface.

A harmonic point load was applied only to one of the tunnels located 40 m below the ground surface, simulating an active rail tunnel, while the second tunnel remained passive. This setup allowed for assessment of structural coupling and energy redistribution caused by the two cavities. As in the single tunnel case, PML were applied to eliminate the reflections.The mesh was refined to ensure at least five elements per wavelength, allowing accurate resolution of wave behavior up to 800 Hz. Vibration responses were evaluated as vertical velocity at surface receiver points and analyzing average velocity levels along surface lines. Results were compared with the single tunnel case to quantify the influence of the second tunnel on wave propagation. The figures below show the twin tunnel in three different configurations, along with the locations of the receiver points on the ground surface 3.5.

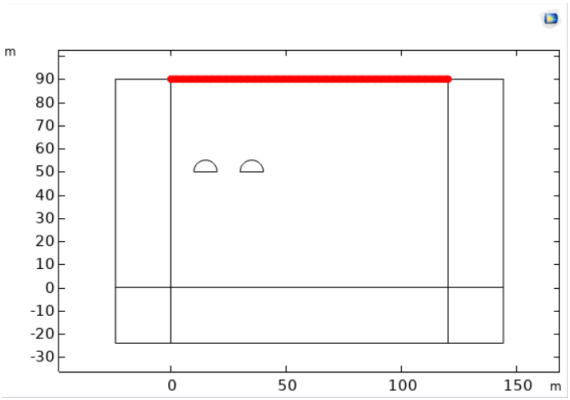

(a) Receiver positions along the ground surface (indicated by the red line) for the side-by-side tunnel configuration

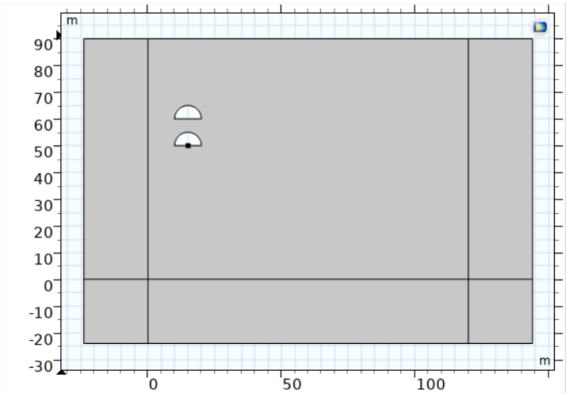

(b) Vertical offset configuration

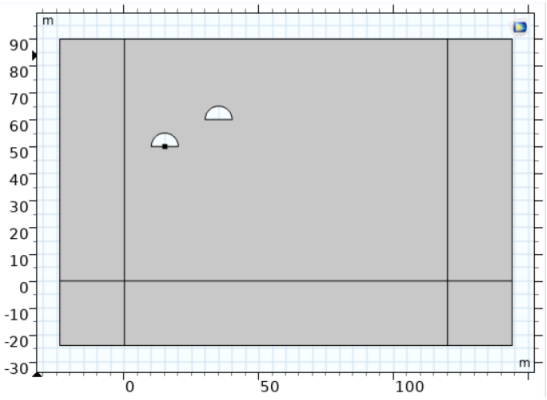

(c) 45-degree configuration

Figure 3.5: Configurations comparison

Directivity analysis

An additional analysis was conducted to examine the directional propagation of ground-borne vibrations from tunnel excitation. The goal was to understand how the presence and layout of a second tunnel affect the angular distribution of vibration energy in the surrounding bedrock. This directivity study complements the general response analysis by highlighting how vibration radiates in different directions from the tunnel system. As in previous simulations, a harmonic vertical point load was applied at the center of the invert of one tunnel to simulate an active railway. The second tunnel remained passive. The simulations were carried out in the frequency domain using the Solid Mechanics interface in COMSOL Multiphysics.

To evaluate angular response, a circular array of receivers was positioned around the tunnel configuration at a fixed radius. Velocity responses were extracted at each point and converted into 1/3-octave band levels. This setup made it possible to assess how vibration amplitude varies with direction across a full 360-degree profile.

To investigate the influence of tunnel configuration on vibration directivity, three twin tunnel arrangements—side-by-side, vertically offset, and 45-degree inclined—were compared to a single tunnel reference. Figure 3.6 illustrates the configurations and the placement of receiver points around the tunnels used to capture wave propagation patterns. These tunnel configurations were chosen because they reflect common layout practices in underground construction projects. This made it possible to compare how different arrangements affect the directionality of wave propagation.

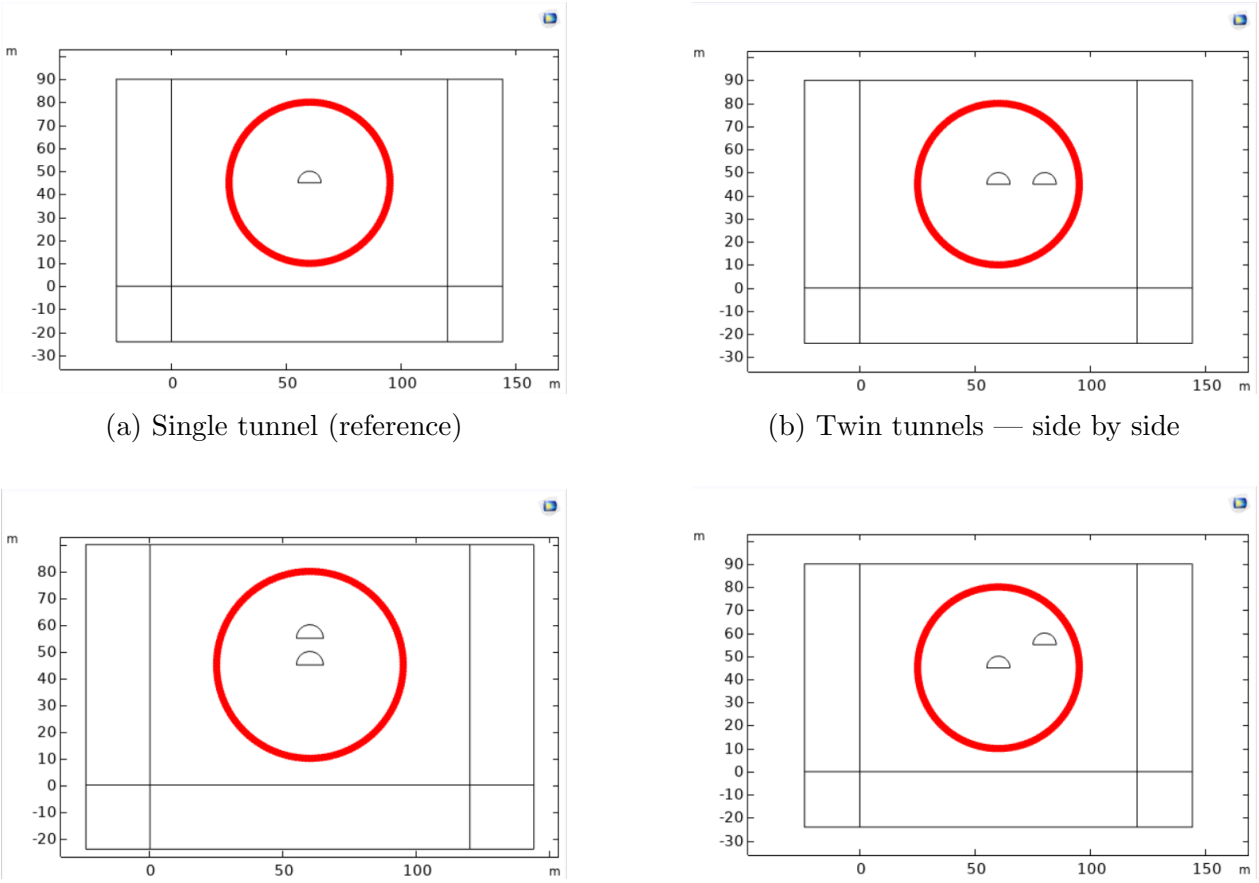

(a) Single tunnel (reference)

(b) Twin tunnels — side by side

(c) Twin tunnels — vertical offset

(d) Twin tunnels — 45-degree configuration

Figure 3.6: The twin tunnel scenarios illustrate how the receivers are positioned around the underground twin tunnels.

3.2.2 Numerical simulation in 3D

Three-dimensional simulations were carried out to complement the 2D analysis by capturing spatial effects, validating 2D trends, and providing a more realistic representation of ground-borne vibration propagation. The 3D domain was defined with a width of 60 m, a height of 50 m, and a depth of 40 m. The tunnel geometry was modeled as a cylindrical cavity with a radius of 5 m, consistent across both single and twin tunnel scenarios to enable direct comparisons.

In the twin tunnel case, two parallel tunnels were positioned side by side with a center-to-center spacing of 20 m, reflecting a typical twin tunnel layout. A point load was applied at the invert of one tunnel, simulating dynamic excitation. No fracture zones were included in the 3D simulations, maintaining consistency with the 2D reference cases. The primary difference between the 2D and 3D models lies in the excitation source: in the 2D model, a point load represents an *coherent line source*, while in the 3D model, it corresponds to a true point source. PMLs were implemented along the domain boundaries to absorb outgoing waves and eliminating the reflections. A frequency-dependent mesh refinement strategy was employed using a parametric sweep, ensuring a minimum of five elements per wavelength across the frequency range of 16 Hz to 400 Hz.

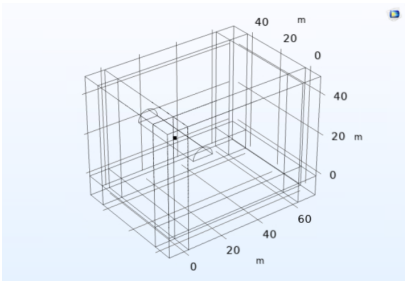

(a) Single tunnel located 25 m underground.

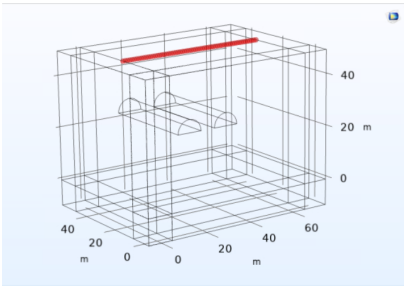

(b) Twin tunnels (side-by-side) with receiver line along the ground surface.

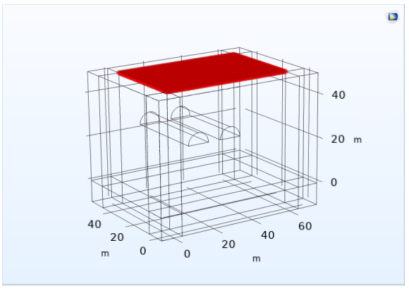

(c) Twin tunnels with the ground surface fully covered by receiver points.

Figure 3.7: 3D tunnel configurations showing receiver placement for simulation analysis.

3.3 Site measurement

To investigate the real-world behavior of ground-borne vibration attenuation, field measurement data were collected on the ground surface above the Gårda tunnel in Gothenburg. The primary aim was to study the attenuation of vertical vibration components induced by rail traffic and to interpret the results in light of the numerical simulation findings.

The measurements were performed on September 2nd, 2021, at the yard of Prospect Hillgatan 10, between 13:28 and 13:58. The site is characterized by exposed bedrock with no sediment cover. Vertical ground vibrations were recorded at six surface locations using Wilcoxon 731 seismometers. The receivers were placed at intervals of approximately 6 m along a line extending about 40 m, starting from a reference point (R0) located directly above the tunnel on a building foundation [9]. The receiver positions are according to the image below 3.8

Figure 3.8: [9]: Receiver positions (A1 to A6), Gårda tunnel below, and building above.

(a) Location A1

(b) Location A2

(c) Location A3

(d) Location A4

(e) Location A5

(f) Location A6

Figure 3.9: Photos of measurement locations A1 to A6 (seismometer positions)

Table 3.1 presents the reported train compositions passing the site during the measurement window. The trains varied in length and weight, with some reaching over 150 tonnes. Although the exact train speeds were not known, the vibration signals from six valid passages were successfully recorded.

The data were processed using one-third octave band FFT of vertical velocity and then averaged across the six passages. Due to variability in train parameters and unknown excitation inputs, only relative comparisons of vibration decay trends were made with the numerical models.

Table 3.1: Reported Train Compositions at Gubbero Tunnel on September 2, 2021.

Date	Time	Train No.	Location	Train Type	Locomotive ID	Length (m)	Weight (t)
2021-09-02	13:17	3053	Gubbero	RST	X61947446104160	74.3	154
2021-09-02	13:38	7360	Gubbero	RST	X12947441232149	49.9	103
2021-09-02	13:42	3052	Gubbero	RST	X61947446104152	74.3	154
2021-09-02	13:47	31032	Gubbero	RST	ETS4336	157.8	306
2021-09-02	13:48	3055	Gubbero	RST	X61947446104178	74.3	154
2021-09-02	13:54	7353	Gubbero	RST	X61947446100424	74.3	154

Chapter 4

Results

This chapter summarizes the results from numerical simulations and field measurements undertaken to explore ground-borne vibration propagation through fractured bedrock and across underground railway tunnels. Results have been designed to match different phases of the study, starting with fracture-related simulations, and progressing through tunnel modeling scenarios to field measurement analysis.

Firstly, the impact of fracture geometry is explored through various configurations with differences in number, spacing, and width for fractures. These configurations are contrasted with a reference case with no fractures in order to compare attenuation effects at the ground level. Secondly, as part of a parametric study, it is determined through simulation whether fracture material property including Young's modulus, density, or Poisson's ratio contributes most significantly towards vibration transfer.

Following sections show results from 2D and 3D tunnel simulation runs. The single tunnel runs serve as a reference and provide a point for comparison, while twin tunnel runs explore wave interaction, shielding and directivity effects. Both configurations are compared on the basis of surface velocity response over an appropriate frequency span.

Last but not least, results from site measurements above the Gårda tunnel are given. Vertical ground velocity decay with distance is discussed and compared qualitatively to numerical results to validate observed attenuation behavior.

4.1 Effect of Fracture in Bedrock

A limited number of frequencies were selected for presentation in this study; however, the frequencies were carefully selected to be representative of low, mid, and high-frequency ranges. The influence of fractures on ground-borne vibration propagation was studied using various fracture configurations. Figures 4.1 and 4.2 show the velocity level along the ground surface for scenarios with different numbers of vertical fractures. The results demonstrate a clear trend: increasing the number of fractures consistently enhances vibration attenuation, particularly at frequencies above 250 Hz. For example, at 1000 Hz, configurations with multiple

fractures (4 to 5 fractures) exhibited approximately 40 to 50 dB lower vibration levels compared to the reference without fractures. The spatial distribution of vibration attenuation along the ground surface also showed frequency-dependent behavior, becoming increasingly evident at higher frequencies. These findings confirm the expectations that fractures effectively reduce vibration energy through wave scattering and reflections.

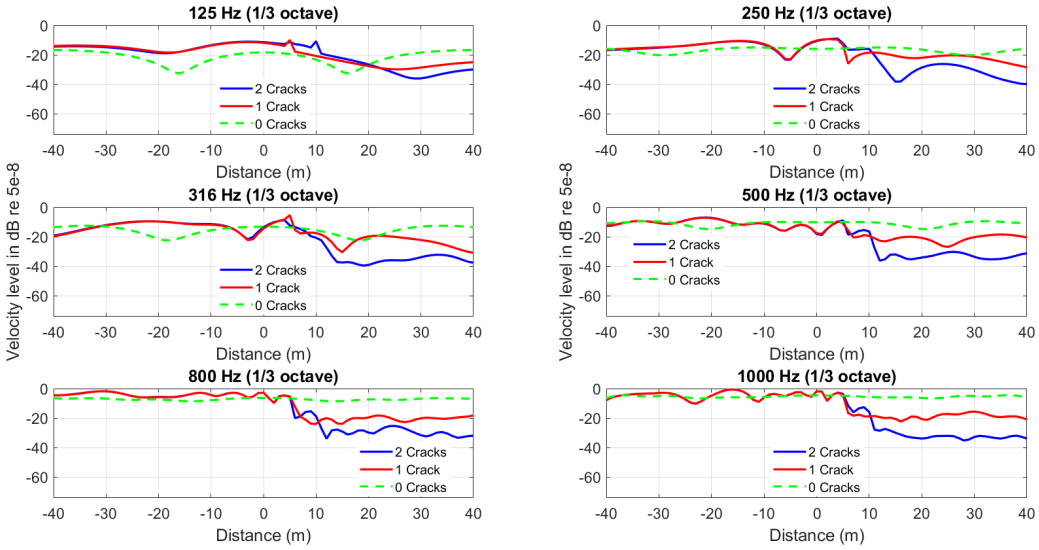

Figure 4.1: Velocity level across the ground surface, ground with 0,1 and 2 cracks

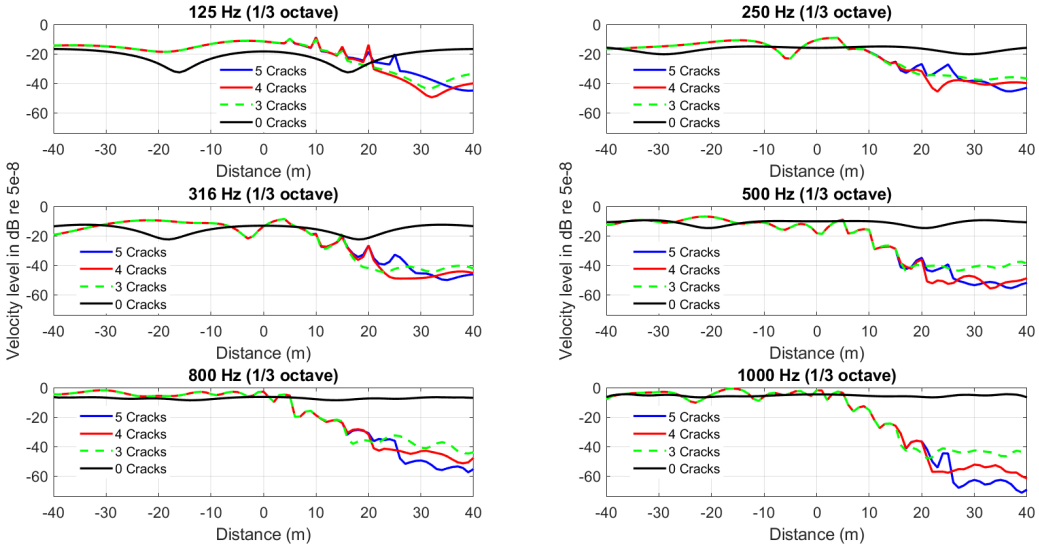

Figure 4.2: Velocity level across the ground surface, ground with 0 crack as reference 3,4 and 5 cracks

The effect of the number of fractures on the velocity level was examined in a receiver located 30 m horizontally away from the source point. The results show a general trend in which the number of fractures (from a single to five fracture zones) successively decreases the level of vibration velocity 4.3a. Another observation is that, in the case of a single and wider fracture zone, the velocity level at mid- and high frequencies - particularly from 125 Hz and upward - decreases less compared to the scenario with multiple fractures. This may be due to fewer wave reflections in the case of a single fracture (Figure 4.3).

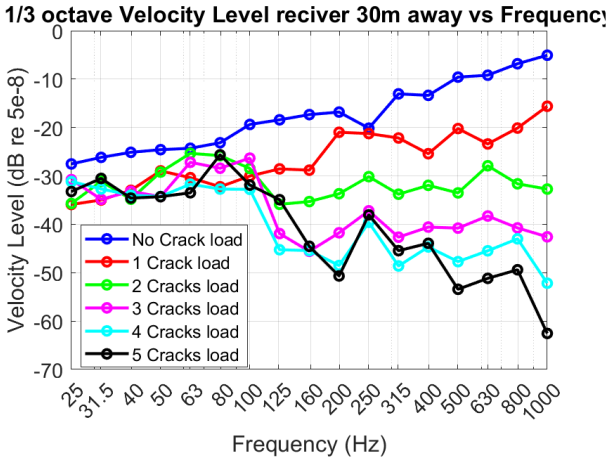

(a) Velocity level with the excitation point 30m underground.

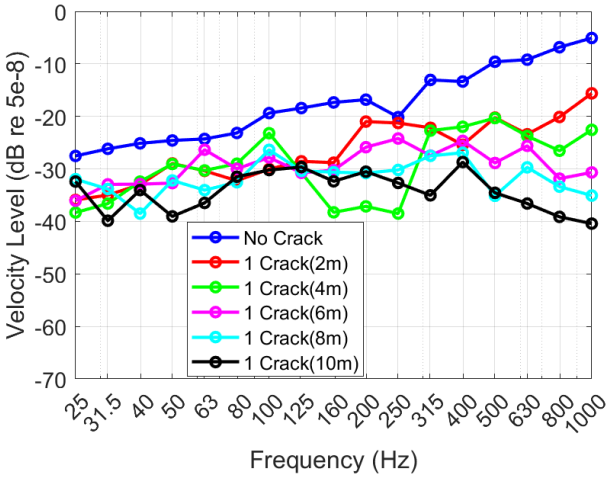

(b) Single crack with a width of 2, 4, 6, 8, and 10 m. excitation point 30m underground.

Figure 4.3: Comparison of surface velocity levels for different crack configurations.

The average velocity levels on the excitation side, measured away from the fractures, display clear and consistent patterns, as shown in Figure 4.4b. When fractures are introduced, the velocity levels increase noticeably across the entire frequency range compared to the no-fracture scenario. This increase is primarily due to vibrations wave being reflected by the fractures back toward the excitation side, resulting in amplified local vibration levels.

Figure 4.4a illustrates the receiver locations on the excitation side, placed at 1-meter intervals along the ground surface of the simulation model from 5 m to 40 m. These receiver points were used to compute the average velocity levels shown in Figure 4.4b.

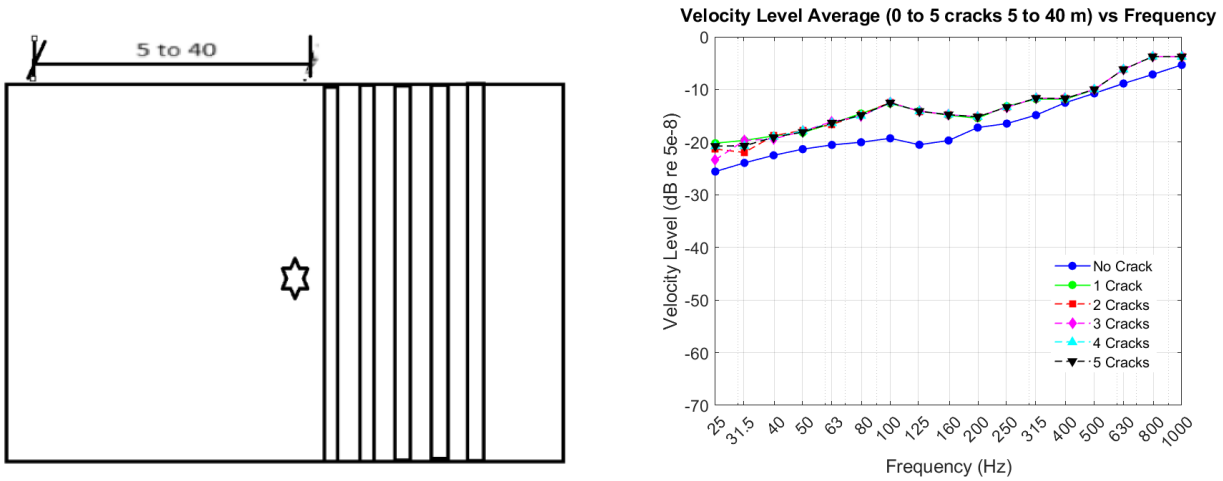

(a) Sketch of the model showing receiver points from 5 m to 40 m on the excitation side in the scenario with multiple fractures.

(b) Average velocity level from 5 m to 40 m on the excitation side with and without fractures.

Figure 4.4: Illustration of spatially averaged velocity levels on the excitation side.

Ground-based velocity level between fractures provided additional information about wave behavior (Figure 4.5). According to predictions, the velocity of vibration gradually reduced by as much as 50 dB with propagation through a series of fractures. However, a further layer of complexity was the reflection patterns and interferences that were present.

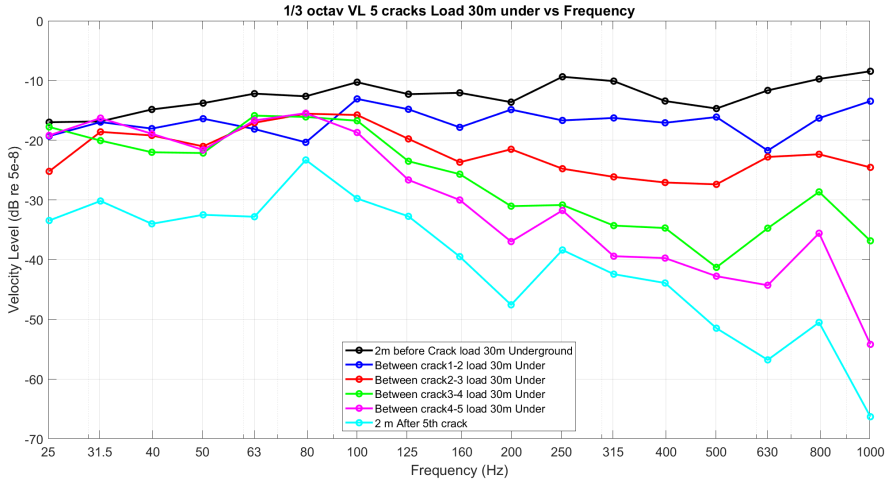

Figure 4.5: Velocity level with the reciver points between each crack in scenario with the 5 cracks

4.1.1 Effect of Fracture Material Properties

Figure 4.6 illustrates how the vibration response is influenced by changes in material properties of cracked rock according to 1/3-octave band analysis. The blue line is for the reference case with a rock density of 1800 kg/m^3, Young's modulus $9 \cdot 10^8$ Pa and Poisson's ratio 0.3,

and a structural loss factor of 0.01. For the other lines, one property is altered at a time while keeping all else constant to see their specific influence separately.

Raising Young's modulus to $9 \cdot 10^9$ Pa (red line) increases velocity levels across most frequencies, particularly below 100 Hz and above 500 Hz. This is expected, as a stiffer material transmits vibrations more effectively. In contrast, increasing the Poisson's ratio to 0.45 (green line) and the density to 2200 kg/m^3 (purple line) has a smaller impact on velocity levels. These curves closely follow the reference line, indicating limited influence from these parameters.

Overall, the results clearly show that **Young's modulus** has the most significant influence on underground vibration propagation. Its effect is more significant compared to the other parameters studied.

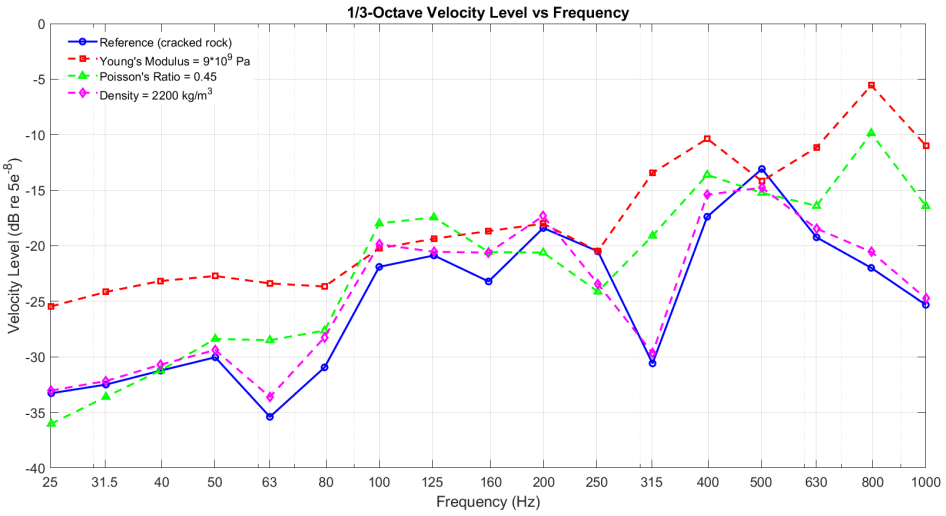

Figure 4.6: Vibration transmission for different fracture material properties.

4.2 2D Tunnel Simulations

4.2.1 Single Tunnel

The spatial variation of vertical velocity levels at the ground surface (Figure 4.7) showed typical attenuation behaviors across different frequencies. In most cases, vibration amplitude gradually decreased with increasing horizontal distance from the tunnel centerline. Lower frequencies (e.g., 25–63 Hz) exhibited smooth and consistent attenuation, while higher frequencies (316–1000 Hz) showed more complex, fluctuating patterns due to their shorter wavelengths and interactions within the bedrock medium.

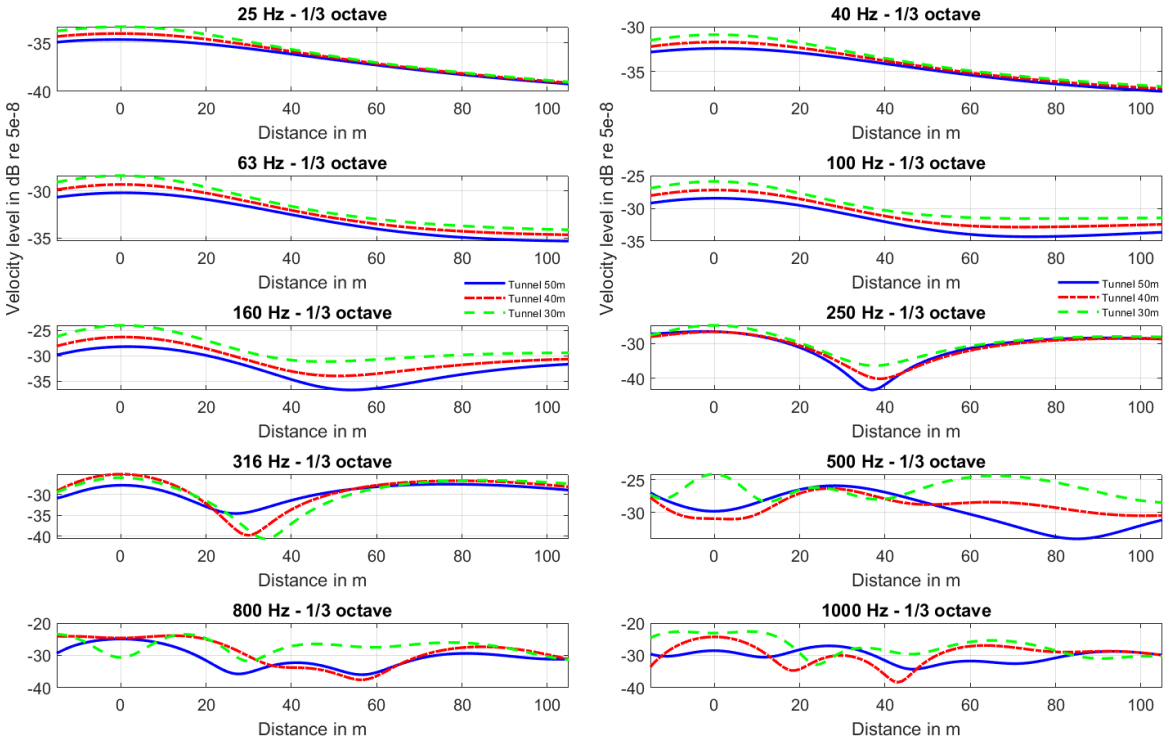

Figure 4.7: Velocity level across the ground surface, when the singel tunnel is 30, 40 and 50m underground

The influence of tunnel depth (Figure 3.4) on surface vibration levels were determined. Surface averaged vertical velocity levels, as measured, receivers positioned 10 to 100 m horizontally from the tunnel centerline, were seen to be dependent on tunnel depth (Figure 4.8). The results reflected uniformly reduced surface vibration levels for deeper tunnels. In particular, the tunnel at 30 m depth displayed considerably higher velocity levels, typically 2–4 dB higher across the frequency range—compared to the tunnels placed at 40 and 50 m depths. This outcome aligns with expectations. This behavior can be explained by Lamb's equation and Bornitz's extension (Equation 2.4), which describe how ground-borne wave amplitudes decay with distance and depth through the ground medium.

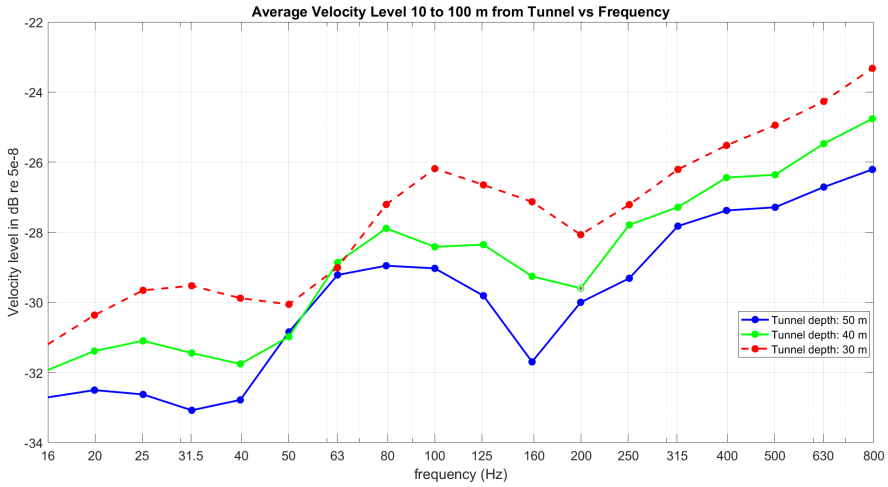

Figure 4.8: Average velocity level from 10 to 100m from tunnel

The velocity level recorded at the receivers is evaluated at horizontal distances of 40, 55, 70, and 90 meters from the tunnel, which is located 30 meters below ground. The simulation results (Figure 4.9) show frequency-dependent vibration attenuation as the propagation distance increases. Notably, the attenuation is not uniform across all frequencies. At lower frequencies (below approximately 100 Hz), the receiver closest to the tunnel (40 m) displays lower velocity levels compared to receivers positioned farther away. This may occur because lower-frequency waves have longer wavelengths, and thus, the closest receiver may not fully register these longer wavelengths when located near the excitation source. Starting from around 100 Hz and upwards, the velocity level at the nearest receiver significantly increases and is noticeably higher than at the more distant receivers. Once again, this result demonstrates that vibration amplitude decays with increasing distance from the source.

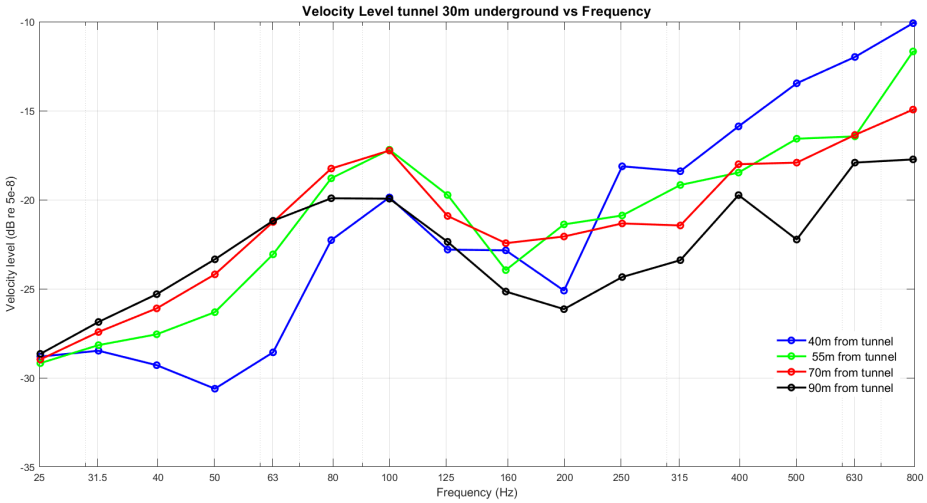

Figure 4.9: Velocity level tunnel 30m underground recivers 40,55,70 and 90m from tunnel at the ground surface

4.2.2 Twin Tunnel

Spatial distribution of velocity levels at the ground surface (Figure 4.10) showed a significant amplification and shielding behaviors. Surface vibration levels varied significantly depending on frequency and tunnel configuration whether side-by-side, vertically aligned, or oriented at 45°—and show complex wave interactions and interference patterns caused by the presence of the secondary tunnel.

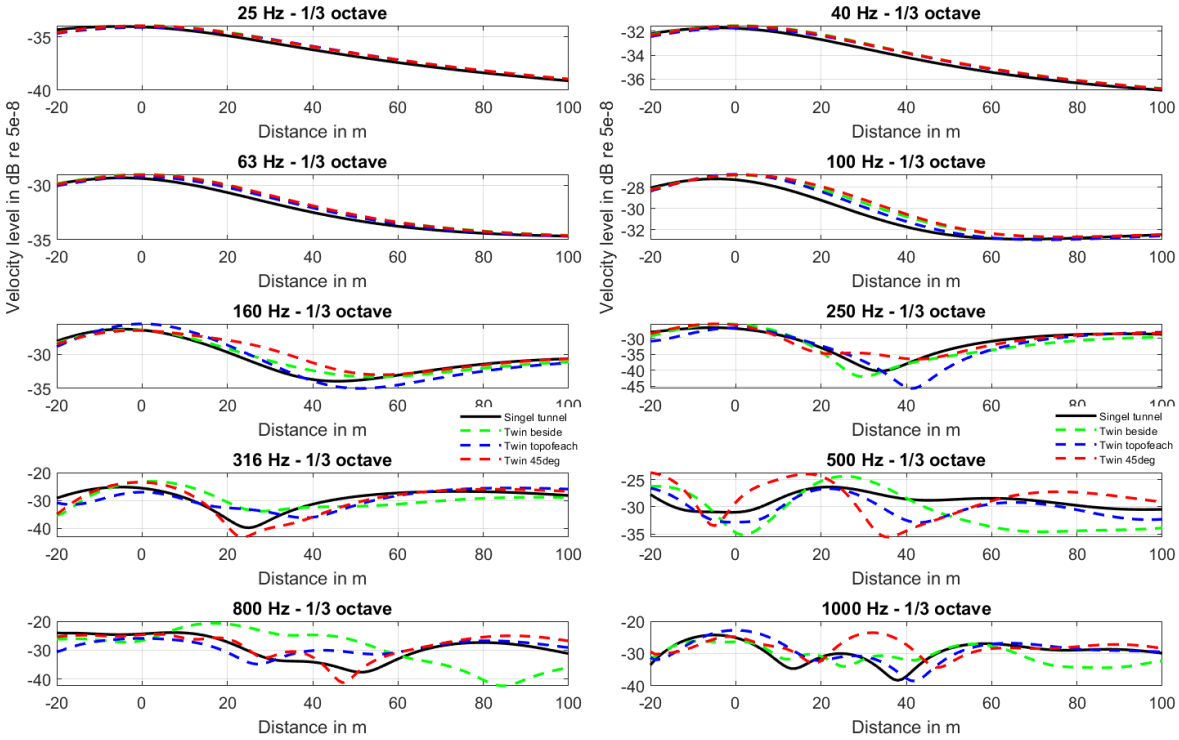

Figure 4.10: Velocity level across the ground surface

The addition of a second tunnel clearly influenced how ground vibrations spread, as demonstrated by comparing twin and single tunnel setups (Figure 4.11). At a point 30 meters horizontally from the source, clear differences were observed, particularly at lower frequencies. Between 31.5 and 63 Hz, the vertically stacked twin tunnels significantly reduced vibration levels compared to the single tunnel scenario. However, since a similar behavior was also observed and explained in the single tunnel case, results above 100 Hz are considered more reliable. Notably, from 125 Hz and upward, the inclined tunnel configuration (at 45°) consistently resulted in 2 to 5 dB lower vibration levels compared to the single tunnel case, particularly in the mid and high-frequency ranges. In contrast, the side-by-side and vertically stacked configurations generally show higher vibration amplitudes within the same frequency range.

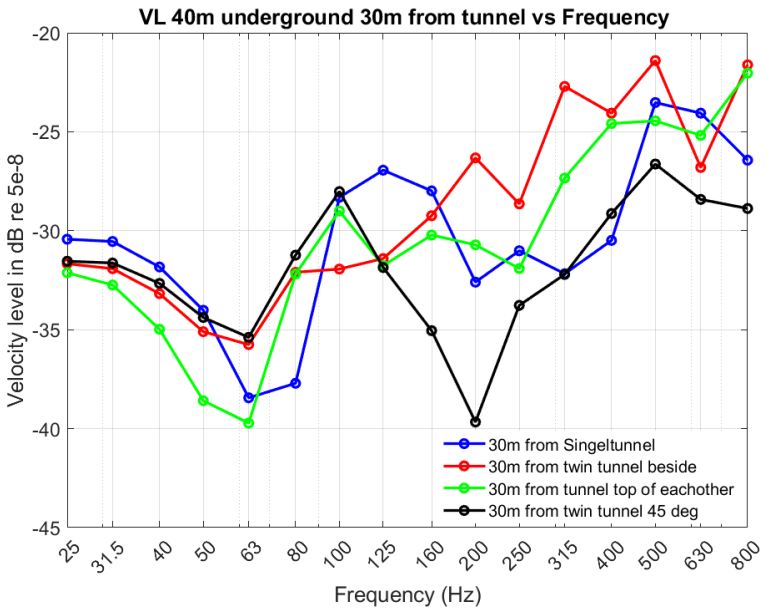

Figure 4.11: Velocity level reciver at 30m from tunnel at the surface

Directivity in Twin Tunnel Scenario

The polar directivity graphs (Figure 4.12) clearly illustrate how vibration propagation varies with direction. Twin tunnel setups show stronger fluctuations in vibration levels, especially near the tunnels and at higher frequencies, compared to the smoother pattern observed for a single tunnel. These pronounced changes are mainly due to complex wave interactions and reflections caused by adding the second tunnel.

In particular, when the tunnels were stacked vertically, vibration levels directly above the tunnels dropped by about 5 to 10 dB. Moreover, at higher frequencies, the 45° inclined tunnel configuration significantly reduced vibrations in the 45° direction, while the side-by-side arrangement reduced vibrations primarily along the tunnel's alignment. However, these directional reductions redistributed vibration energy to other areas, resulting in higher surface levels in some directions.

In general, these results confirm that tunnel geometry plays an important role in affecting ground vibrations as well as directivity, and provide valuable insights for effective design of mitigation strategies in underground railway systems.

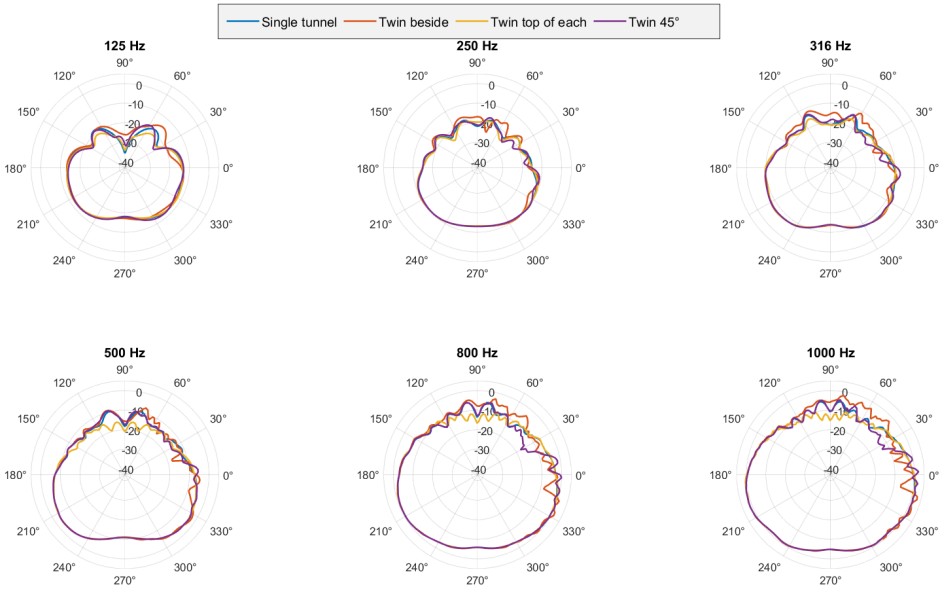

Figure 4.12: Polar directivity plots for twin tunnels with different configurations, compared to a single-tunnel reference.

4.3 3D Tunnel Simulations

To confirm and expand upon the results from the 2D simulations, a corresponding set of 3D models was developed using the same material properties and tunnel geometries. Both a single tunnel and a twin tunnel configuration (with the tunnels placed side by side) were modeled at a depth of 25 m below the ground surface. Excitation was applied as a vertical point load at the tunnel invert, which differs from the 2D simulation setup where the load was modeled as an coherent line source, while in 3D it was modeled as a point source.

Due to computational limitations, the 3D simulations were restricted to a maximum frequency of 400 Hz and used a smaller model domain compared to the 2D simulations. In contrast, the 2D models extended up to 800 Hz and had a domain size at least twice as large. Velocity levels were evaluated at the ground surface, including single-receiver measurements at 20 m from the tunnel centerline, as well as spatial averages between 5–15 m away. The results showed good agreement between the 2D and 3D simulations in both overall trends and frequency-dependent behavior, as illustrated in Figure 4.13a and Figure 4.13b.

As expected, the 3D simulations showed lower velocity levels due to wave energy being distributed in three dimensions, while the 2D models confined the energy within a plane, resulting in higher surface amplitudes 4.13a. However, the difference between single and twin tunnel cases within this frequency range was relatively small. The 3D surface plots (Figures 4.14 and 4.15) confirmed similar trends between the configurations.

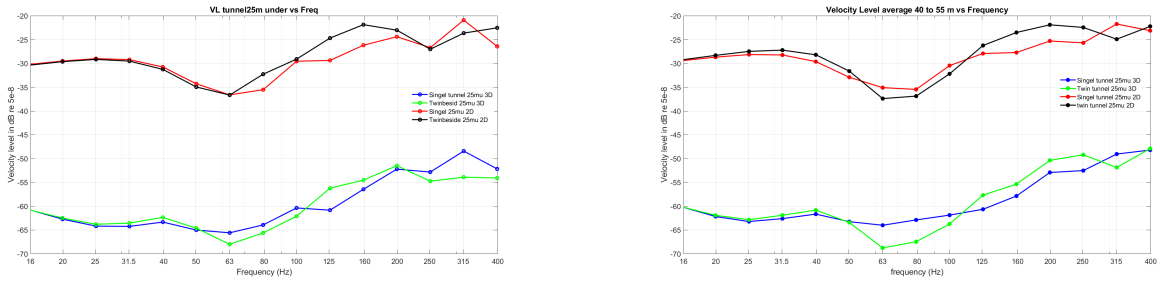

(a) Velocity level comparison at a single receiver (e.g., 20 m from the tunnel).

(b) Average velocity levels over receivers from 5 m to 15 m.

Figure 4.13: Comparison between 2D and 3D simulations of velocity levels at the surface for different receiver configurations.

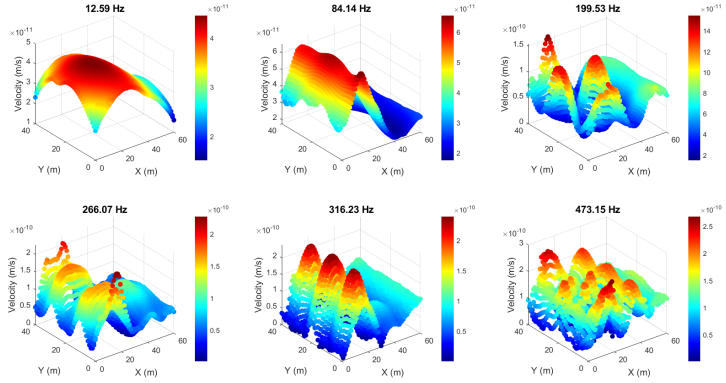

Figure 4.14: Velocity level at the ground surface Singel tunnel

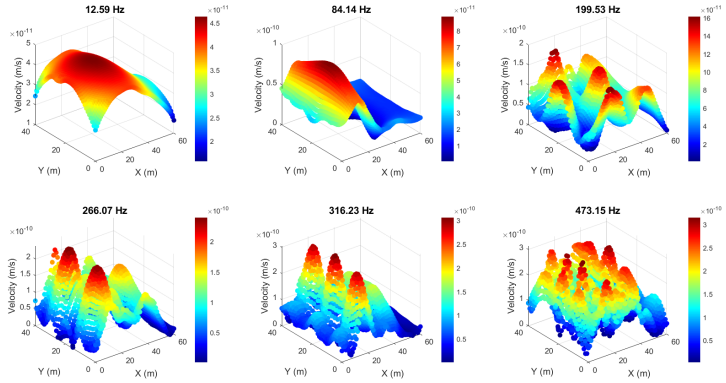

Figure 4.15: Velocity level at the ground surface Twin tunnel

4.4 Site Measurement Results

Figures 4.18–4.23 show the 1/3-octave band velocity spectra at each of the six surface positions, based on six train passages. Although some variation is observed between passages likely due to differences in train speed, weight, and length the general spectral shape is consistent across all positions. Most positions exhibit a prominent peak in the frequency range between 250–400 Hz, which is in line with the dominant frequency range observed in the simulation results for bedrock.

To reduce variability caused by unknown operational parameters, such as speed of the train, an average spectrum across all six passages was calculated for each position. These are shown in Figure 4.24. Although the train type remained the same for each passage, variations in length, weight, and speed justified the use of averaged values.

The general pattern shows a slight reduction in velocity levels with increasing distance, though the decrease is not strictly uniform. Notably, Position 2 records the highest levels, which is unexpected based on distance alone. This may be due to the local quality of the bedrock, local ground coupling effects (e.g. influence of foundations or the effect of the steep slope of the bedrock surface), or measurement error (e.g. transducer not attached firmly enough to the bedrock). There is no measurement twice verification as the measurements were not repeated.

The full-position average (Figure 4.24) further confirms a spectral peak between 250–400 Hz, followed by a consistent decline in levels beyond 500 Hz. This supports the hypothesis that vibration attenuation in bedrock is more significant in the mid-to-high frequency range. At lower frequencies, the longer wavelengths tend to bend around hindrance and pass through the medium with less resistance. In contrast, mid and high frequencies, with shorter wavelengths, are more sensitive to material discontinuities, resulting in greater energy loss and increased reflections.

The A-weighted velocity spectra for Passage 1 (Figure 4.16) reflect similar trends, with Position 2 again showing slightly elevated levels. Despite such local variations, the overall pattern remains stable across positions, reinforcing the existence of a dominant frequency band where vibration energy is concentrated.

Time-domain results (Figure 4.17) reveal slight differences in arrival time between positions. Peak amplitudes are greatest at the first few locations and gradually decrease with distance, indicating attenuation along the propagation path. However, the decay is irregular, likely due to local geological variations or wave reflections.

Overall, the field measurement results confirm the key trends observed in the simulation study:

- Dominant vibration frequencies in bedrock lie between 250–400 Hz.
- Surface velocity levels generally decrease with distance from the source, though not uniformly.
- Vibration energy attenuates more rapidly beyond 500 Hz, consistent with frequency-

dependent damping.

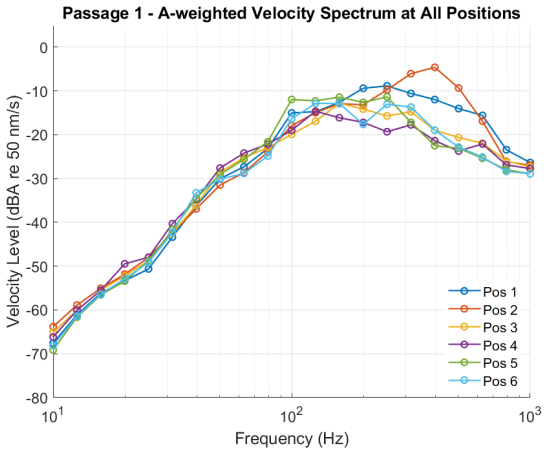

Figure 4.16: 1/3-octave velocity spectrum at the ground surface.

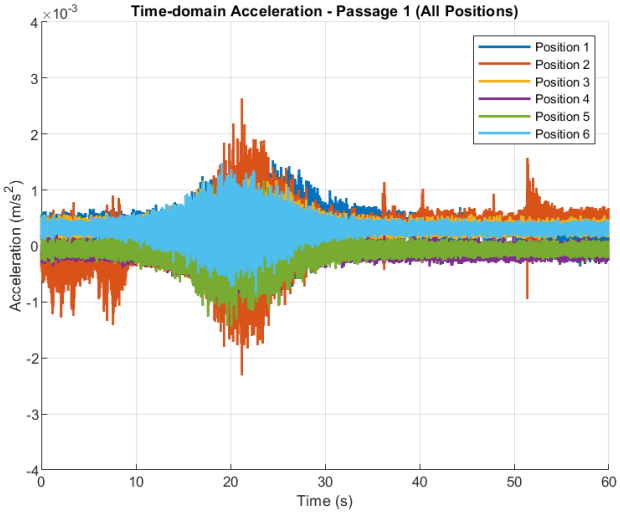

Figure 4.17: Time-domain acceleration at the ground surface.

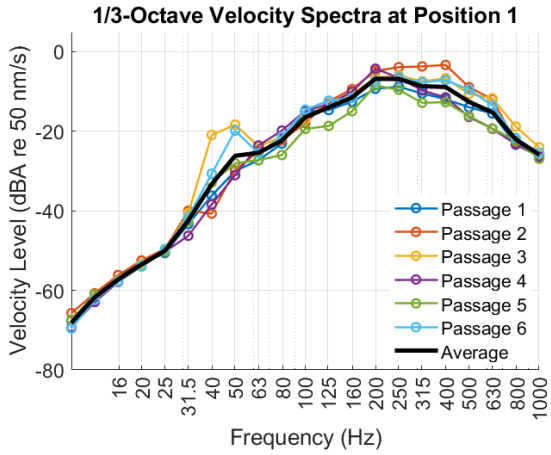

Figure 4.18: A-weighted 1/3-octave velocity at Position 1 (all passages).

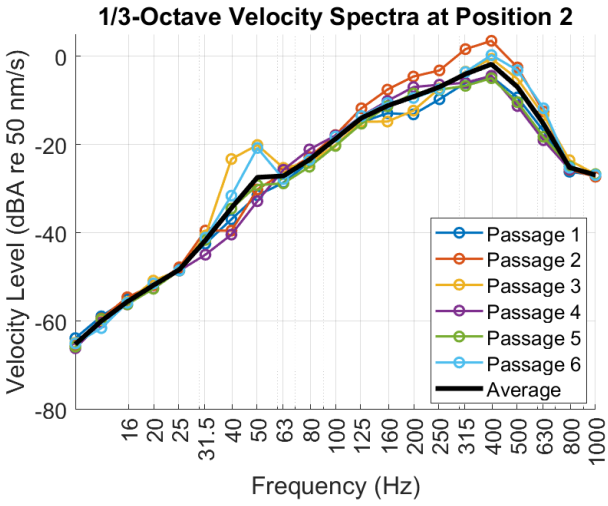

Figure 4.19: A-weighted 1/3-octave velocity at Position 2 (all passages).

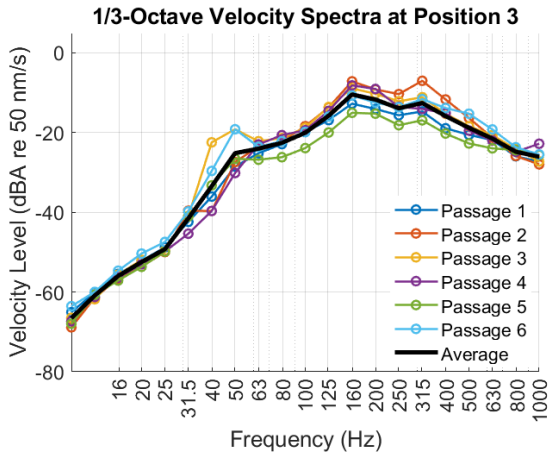

Figure 4.20: A-weighted 1/3-octave velocity at Position 3 (all passages).

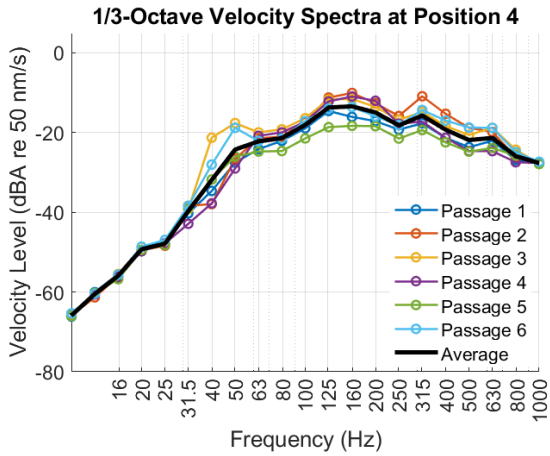

Figure 4.21: A-weighted 1/3-octave velocity at Position 4 (all passages).

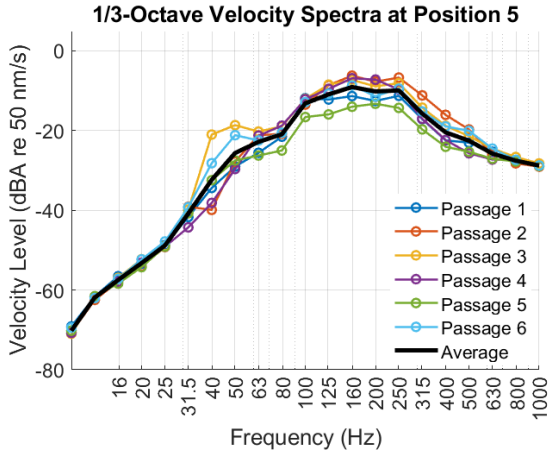

Figure 4.22: A-weighted 1/3-octave velocity at Position 5 (all passages).

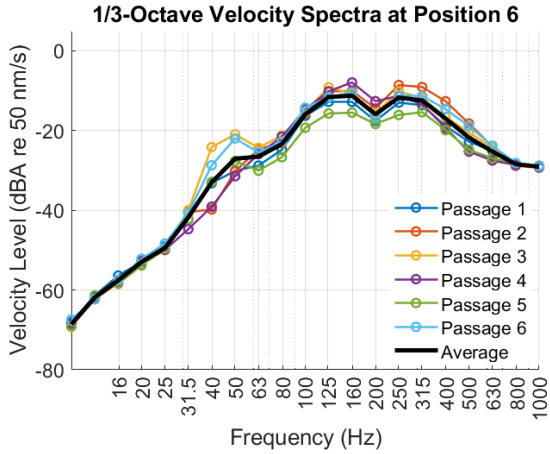

Figure 4.23: A-weighted 1/3-octave velocity at Position 6 (all passages).

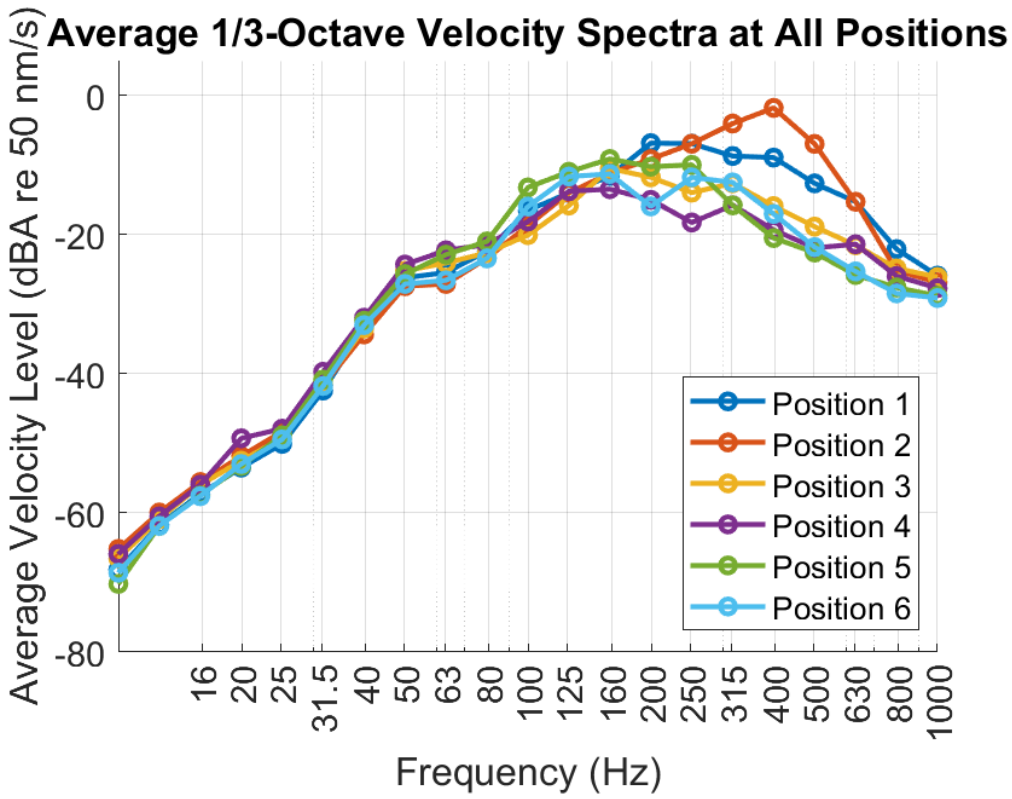

Figure 4.24: Average A-weighted 1/3-octave velocity spectra for Passage 1 (Positions 1–6).

Chapter 5

Discussion

This MSc project numerically investigated ground borne vibration propagation from tunnels in bedrock, focusing specifically on the influence of fracture zones, tunnel geometry, and dimensionality (2D vs. 3D simulations). Numerical simulations revealed that parameters such as fractures significantly impact vibration attenuation, confirming that detailed geological characterization is essential. The findings were further strengthened by comparison with field measurement data, demonstrating that the numerical approach reliably captured the primary trends observed at a site with similar geological conditions.

5.1 Impact of Fractures on Vibration Transmission

The simulation results clearly show that fracture zones in bedrock significantly influence the attenuation of ground-borne vibrations. As illustrated in Figure 4.3a, increasing the number of fractures reduces surface velocity levels, especially within the mid-to-high frequency range (100–800 Hz). This effect is consistent both at individual receiver positions (e.g., 30 m from the source) and when averaging velocities across multiple positions on the surface (200–800 Hz range).

As illustrated in Figure 4.5, velocity measurements taken between fracture zones reveal additional localized reflections, leading to irregular patterns of decay. These behaviors are both frequency-dependent and spatially complex, aligning with previous research on wave propagation in fractured geological media.

In contrast, when analyzing a single fracture zone with varying widths (from 2 m to 10 m), the reduction in surface velocity was less significant compared to the multiple fracture case (Figure 4.3b). This may be due to the limited number of wave reflections occurring in the single-zone scenario, which reduces the overall scattering effect.

The observed increase in vibration levels on the side of excitation clearly shows how fractures significantly affect wave propagation by acting as reflective barriers. As illustrated in Figure 4.4b, these fractures strongly reflect vibrational waves, especially at lower frequencies where the wavelengths are longer. This reflection enhances wave interactions, leading to more

pronounced vibrations. This behavior aligns well with established wave propagation theories and highlights why it's crucial to account for reflections caused by fractures when predicting vibrations. Future models should pay special attention to these reflective effects in fractured geological formations, as they can greatly impact vibration levels close to the source.

5.2 Effect of Tunnel Depth on Surface Vibrations

Tunnel depth significantly influences surface vibration levels. Figures 4.8 and 4.7 clearly illustrate that shallower tunnels produce higher average surface velocities, with differences ranging between approximately 2 and 4 dB across the considered frequency range. This is expected since shallower tunnels reduce the distance waves must travel, thus minimizing material damping and distance attenuation due to spread of the wave energy.

However, as shown in Figure 4.9, The results confirm a clear link between receiver distance and vibration attenuation, aligning with theory. Higher frequencies show stronger decay with distance, while lower frequencies (25–100 Hz) reveal irregular patterns, likely caused by wave interference or reflections near the source, which may explain the lower velocity at 40 m. At mid frequencies (125–160 Hz), curves from all receivers merge, suggesting uniform wave behavior across distances. Beyond this range, attenuation increases steadily. These patterns highlight the importance of considering wave interference and rock properties in modeling, and they support the reliability of the simulation in capturing realistic ground-borne vibration behavior.

5.3 Influence of Tunnel Geometry and Twin Configurations

Several twin-tunnel layouts were analyzed to understand their effect on surface vibrations at a tunnel depth of 40 m. Comparing twin-tunnel scenarios to the single-tunnel reference (Figure 4.11) showed notable variations in surface vibration levels and their spatial distribution. Specifically, the 45° tunnel arrangement reduced surface vibrations by approximately 3–7 dB at particular frequencies, likely due to wave interference and reflections between tunnel walls. However, no uniform trend emerged across all frequencies.

The spatial attenuation patterns presented in Figure 4.10 further underline the importance of tunnel geometry. At higher frequencies, velocity curves showed pronounced fluctuations, demonstrating increased sensitivity to tunnel layout and resulting wave interactions. Notably, the vertically stacked tunnel configuration provided substantial vibration reduction directly above the tunnels, whereas the side-by-side configuration reduced vibrations more effectively at greater horizontal distances (around 50 m and beyond). These insights suggest that careful consideration of tunnel geometry as while an additional tunnel may reduce vibrations "behind" it, vibration in other directions may be increased.

Polar directivity analysis (Figure 3.6) reinforced these observations, highlighting geometry-dependent angular distributions of vibration energy. The vertically stacked tunnels resulted in significant vibration reductions above the tunnel, attributed to constructive interference

and wave cancellation. Conversely, the side-by-side arrangement caused greater vibration attenuation on the side adjacent to the second tunnel, indicative of reflections and energy redistribution effects.

5.4 2D vs. 3D Simulation Comparison

Although 2D simulations were widely used for their computational efficiency, selected 3D simulations were conducted to validate the results. As shown in Figures 4.13a and 4.13, both approaches displayed similar frequency-dependent trends. However, the 3D simulations consistently produced lower absolute velocity levels, which is expected due to the additional energy spreading in three-dimensional space.

The 3D surface plots (Figures 4.14 and 4.15) revealed greater spatial variability particularly at higher frequencies capturing realistic wave scattering and directional effects that 2D models cannot fully represent.

5.5 Site Measurements

Averaged spectra (Figure 4.24) demonstrated clear mid-frequency dominance and significant attenuation above 600 Hz, with vibration levels generally decreasing at more distant receiver positions. Additionally, time-domain acceleration data (Figure 4.17) confirmed a general reduction in amplitude with increasing distance from the tunnel. However, the decay was not uniformly linear, notably at Position 2, which exhibited unexpectedly higher vibration levels in both frequency and time domains. This anomaly is likely related to local geological or measurement-specific conditions.

Chapter 6

Conclusion

This thesis investigated ground-borne vibration transmission from underground railway tunnels in bedrock, focusing on the effects of fracture zones, tunnel geometry, and model dimensionality. The study combined numerical simulations using COMSOL Multiphysics with field measurements to better understand how vibrations propagate in stiff ground conditions.

The results clearly demonstrated that fractures in the bedrock play a significant role in vibration attenuation, particularly in the mid-to-high frequency range. As the number or width of fracture zones increased, surface velocity levels decreased due to enhanced wave scattering and energy dissipation. The simulations also showed that tunnel depth influence surface vibration levels, with deeper tunnels producing lower amplitudes due to longer propagation paths and increased material damping.

Twin tunnel configurations were found to affect both the magnitude and direction of vibration propagation. While the presence of a second tunnel introduced more complex interference patterns, the resulting surface vibration levels varied noticeably depending on the specific tunnel layout and receiver location. Specifically, an additional tunnel generally provided attenuation in vibration levels behind it, whereas amplification of vibrations could occur in other directions or positions relative to the tunnels.

Comparison between 2D and 3D simulations revealed consistent trends in frequency response, though 3D models more accurately captured spatial variability and wave directionality due to energy distribution in three dimensions.

Field measurements supported the main simulation outcomes: dominant vibration frequencies were observed between 250–500 Hz, and surface amplitudes generally decreased with horizontal distance from the tunnel. Despite some local variability, the strong agreement between measurements and simulations confirms the reliability of the numerical modeling approach.

Overall, these findings provide valuable insights for evaluating ground-borne vibration in bedrock environments and emphasize the importance of accounting for geological features and tunnel design in predictive analyses.

6.1 Future work

The modeling of fractured bedrock could be further improved by incorporating fractures with different orientations and the presence of fluid-filled zones, allowing for a more realistic representation of subsurface conditions. With increased computational resources, future research could also explore higher frequency ranges in 3D simulations and include more complex geological geometries.

In addition, analyzing site measurement data from multiple locations with similar ground properties and consistent receiver placement would improve understanding of subsurface wave behavior. Collecting more detailed geotechnical information about the site would also help align the numerical model more closely with real-world conditions.

Bibliography

[1] N. Barton, R. Lien, and J. Lunde. "Engineering classification of rock masses for the design of tunnel support". In: *Rock Mechanics* 6.4 (1974), pp. 189–236.

[2] Jean-Pierre Berenger. "A Perfectly Matched Layer for the Absorption of Electromagnetic Waves". In: *Journal of Computational Physics* 114.2 (Oct. 1994), pp. 185–200.

[3] L. Bergmann, H. Hatfield, et al. *Ultrasonics and their scientific and technical applications*. 1938.

[4] Z. T. Bieniawski. *Rock Mass Classification*. Wiley, 1978.

[5] F. K. Boadu and L. T. Long. "Wavelet-based detection of rock fractures". In: *Geophysical Research Letters* 23.24 (1996), pp. 3543–3546.

[6] M. Cai and J. Zhao. "Estimation of rock joint stiffness and its effect on wave propagation". In: *International Journal of Rock Mechanics and Mining Sciences* 37.5 (2000), pp. 831–842.

[7] Campbell Associates. *Peak Particle Velocity – Why Do We Monitor It?* `https://campbell-associates.co.uk/peak-particle-velocity-why-do-we-monitor-it/`. Accessed: 2025-06-30. 2024.

[8] European Commission. *Environmental Noise Directive*. Retrieved on 2024-12-19. 2022. URL: `https://environment.ec.europa.eu/topics/noise/environmental-noise-directive_en`.

[9] Fatemeh Dashti. *A Ground-Borne Noise Prediction Model for Railway Traffic in Tunnels in Bedrock*. 2023. URL: `https://www.chalmers.se`.

[10] Harry Thomas Holmes. *Modelling high-speed rail induced vibrations around tunnels (jointed rock masses)*. 2023.

[11] Tommaso Meinardi. *Numerical Prediction of Ground-Borne Vibrations on a Building*. Relator: Prof. Cecilia Surace, Prof. Jean-Marc Battini; Co-Relator: Dott. Marco Civera, Dott. Abbas Zangeneh Kamali. 2023.

[12] Jim Nordström. *Empirical Prediction of Ground-Borne Vibration from Railway Systems: Validating the HS2 model in Sweden, west coast*. 2022. URL: `https://www.chalmers.se`.

[13] L. J. Pyrak-Nolte, L. R. Myer, and N. G. W. Cook. "Transmission of seismic waves across single natural fractures". In: *Journal of Geophysical Research: Solid Earth* 95.B6 (1990), pp. 8617–8638.

[14] P.K. Singh & M.P. Roy. *Damage to surface structures due to blast vibration*. 2010. DOI: https://www.sciencedirect.com/science/article/pii/S1365160910001073.

[15] Sumit Shoor and Manpreet Singh. "Modal and Static Analysis for Analyzing the Effect of Loading on Crack Propagation Rate Using FEM". In: *Recent Trends in Industrial and Production Engineering*. Ed. by A. K. Dubey et al. Lecture Notes in Mechanical Engineering. Singapore: Springer Nature Singapore, 2022, pp. 155–171. DOI: 10.1007/978-981-16-3135-1_17.

[16] E. Taniguchi and K. Sawada. "Attenuation with distance of traffic-induced vibrations". In: *Soils and Foundations* 19.2 (1979), pp. 15–28.

[17] David Thompson. *Railway Noise and Vibration: Mechanisms, Modelling and Means of Control*. Oxford, UK: Elsevier, 2009. ISBN: 978-0-08-045147-3.

[18] Trafikverket. *Buller och vibrationer från trafik på väg och järnväg*. 2024. DOI: http://dx.doi.org/10.1002/andp.19053221004.

[19] Author Unknown. "Holmes Tunnel Vibrations". In: *Internal Report or Thesis* (Unknown).

[20] Paul de Vos and Satis. *RAILWAY INDUCED VIBRATION State of the art report*. Retrieved on 2024-12-19. 2017. URL: https://uic.org/IMG/pdf/uic-railway-induced-vibration-report-2017.pdf.

[21] R. D. Woods and L. P. Jedele. *Energy–attenuation relationships from construction vibrations*. 1985.

[22] J. Zhao and M. Cai. "Transmission and reflection of plane waves across rock joints". In: *International Journal of Rock Mechanics and Mining Sciences* 43.5 (2006), pp. 776–788.